REPORT NO. DOT-TSC-OST-78-1

EXPERIMENTAL INVESTIGATION OF AERODYNAMIC CHARACTERISTICS OF A TRACKED RAM AIR CUSHION VEHICLE

H.C. Curtiss, Jr.
W.F. Putman

Princeton University
Department of Aerospace
and Mechanical Sciences
Princeton NJ 08540

JANUARY 1978

INTERIM REPORT

DOCUMENT IS AVAILABLE TO THE U.S. PUBLIC THROUGH THE NATIONAL TECHNICAL INFORMATION SERVICE, SPRINGFIELD, VIRGINIA 22161

Prepared for
U.S. DEPARTMENT OF TRANSPORTATION
OFFICE OF THE SECRETARY
Office of the Assistant Secretary
for Systems Development and Technology
Office of Systems Engineering
Washington DC 20590

Technical Report Documentation Page

1. Report No.	2. Government Accession No.	3. Recipient's Catalog No.
DOT-TSC-OST-78-1		

4. Title and Subtitle	5. Report Date
EXPERIMENTAL INVESTIGATION OF AERODYNAMIC CHARACTERISTICS OF A TRACKED RAM AIR CUSHION VEHICLE	January 1978
	6. Performing Organization Code

7. Author(s)	8. Performing Organization Report No.
H. C. Curtiss, Jr., and W. F. Putman	DOT-TSC-OST-77-35 AMS Technical Report 1318

9. Performing Organization Name and Address	10. Work Unit No. (TRAIS)
Princeton University* Department of Aerospace and Mechanical Sciences Princeton NJ 08540	OS763/R8513
	11. Contract or Grant No. DOT-TSC-682

12. Sponsoring Agency Name and Address	13. Type of Report and Period Covered
U.S. Department of Transportation Office of the Secretary, Office of Assistant Secretary for Systems Development and Technology. Office of Systems Engineering. Washington DC 20590	INTERIM REPORT Sep. 1973 - Dec. 1976
	14. Sponsoring Agency Code

15. Supplementary Notes *Under Contract to: U. S. Department of Transportation
Transportation Systems Center
Kendall Square
Cambridge MA 02142

16. Abstract

The results of an experimental and theoretical investigation of the longitudinal aerodynamic characteristics of a tracked ram air cushion vehicle are presented. Experiments have been conducted both in a wind tunnel with a model and section of guideway and with the same model propelled along a 300-foot guideway. Experimental results are presented for the dependence of the lift, drag, and pitching moment of the model on model height above the guideway and winglet gap, providing basic data necessary for the analysis of longitudinal stability and ride qualities of the concept. The stability derivatives determined from the moving-model experiments have agreed well with the wind tunnel results. A theory is presented which shows good agreement with the experimental results for the stability derivatives.

17. Key Words	18. Distribution Statement
High-Speed Ground Transportation Ram Air Cushion Ram Wing Aerodynamic Lift	DOCUMENT IS AVAILABLE TO THE U.S. PUBLIC THROUGH THE NATIONAL TECHNICAL INFORMATION SERVICE, SPRINGFIELD, VIRGINIA 22161

19. Security Classif. (of this report)	20. Security Classif. (of this page)	21. No. of Pages	22. Price
UNCLASSIFIED	UNCLASSIFIED	112	

Form DOT F 1700.7 (8-72) Reproduction of completed page authorized

PREFACE

Research into the possibility of using aerodynamic lift for application to ground transportation vehicles has been carried out at a very low level for approximately 10 years. This has been limited to simple analytical investigations and small-scale experiments. During this time, the concept has gone through considerable evolution beginning with a simple body designed to travel through a tube and reaching the stage of a vehicle traveling in an open guideway with flexibly mounted winglets.

In 1973, a system definition study was completed which described the characteristics of a 300-mph intercity system. This study revealed a small requirement of suspension power relative to alternative non-contact suspension schemes, plus a potential for low guideway cost due to the large average gap. Because of these favorable characteristics, the present study was initiated to establish experimentally the dynamic properties of the concept.

Funding was initially provided by the Federal Railroad Administration (FRA) under the Electric Power and Propulsion for High-Speed Tracked Vehicles program. More recently, funding was provided by the Office of the Secretary of Transportation (OST) under the Transportation Advanced Research Projects (TARP) program. Further experiments are underway to provide dynamic information which can be used for purposes of comparison with alternative suspension concepts.

METRIC CONVERSION FACTORS

Approximate Conversions to Metric Measures

Symbol	When You Know	Multiply by	To Find	Symbol
		LENGTH		
in	inches	2.5	centimeters	cm
ft	feet	30	centimeters	cm
yd	yards	0.9	meters	m
mi	miles	1.6	kilometers	km
		AREA		
in^2	square inches	6.5	square centimeters	cm^2
ft^2	square feet	0.09	square meters	m^2
yd^2	square yards	0.8	square meters	m^2
mi^2	square miles	2.6	square kilometers	km^2
	acres	0.4	hectares	ha
		MASS (weight)		
oz	ounces	28	grams	g
lb	pounds	0.45	kilograms	kg
	short tons (2000 lb)	0.9	tonnes	t
		VOLUME		
tsp	teaspoons	5	milliliters	ml
Tbsp	tablespoons	15	milliliters	ml
fl oz	fluid ounces	30	milliliters	ml
c	cups	0.24	liters	l
pt	pints	0.47	liters	l
qt	quarts	0.95	liters	l
gal	gallons	3.8	liters	l
ft^3	cubic feet	0.03	cubic meters	m^3
yd^3	cubic yards	0.76	cubic meters	m^3
		TEMPERATURE (exact)		
°F	Fahrenheit temperature	5/9 (after subtracting 32)	Celsius temperature	°C

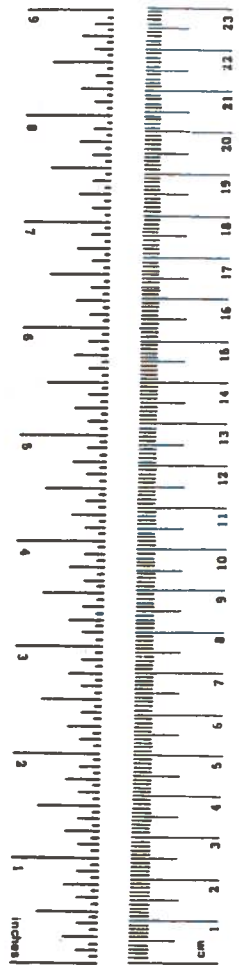

Approximate Conversions from Metric Measures

Symbol	When You Know	Multiply by	To Find	Symbol
		LENGTH		
mm	millimeters	0.04	inches	in
cm	centimeters	0.4	inches	in
m	meters	3.3	feet	ft
m	meters	1.1	yards	yd
km	kilometers	0.6	miles	mi
		AREA		
cm^2	square centimeters	0.16	square inches	in^2
m^2	square meters	1.2	square yards	yd^2
km^2	square kilometers	0.4	square miles	mi^2
ha	hectares (10,000 m^2)	2.5	acres	
		MASS (weight)		
g	grams	0.035	ounces	oz
kg	kilograms	2.2	pounds	lb
t	tonnes (1000 kg)	1.1	short tons	
		VOLUME		
ml	milliliters	0.03	fluid ounces	fl oz
l	liters	2.1	pints	pt
l	liters	1.06	quarts	qt
l	liters	0.26	gallons	gal
m^3	cubic meters	35	cubic feet	ft^3
m^3	cubic meters	1.3	cubic yards	yd^3
		TEMPERATURE (exact)		
°C	Celsius temperature	9/5 (then add 32)	Fahrenheit temperature	°F

TABLE OF CONTENTS

ILLUSTRATIONS

ILLUSTRATIONS (Concl'd)

NOMENCLATURE

a	number of weights aft, (p. 45)
$\bar{A}$	ratio of local area to exit area, $\bar{A} = \frac{A_L}{A_E}$
A_E	area between vehicle and guideway at the vehicle trailing edge, ft^2
A_L	area between vehicle and guideway at any chordwise location, ft^2, $A_L(c) = A_E$
A_{SE}	area between sides of vehicle and guideway at the model trailing edge, $A_{SE} = 7.25$ in.^{2}
c	length or chord of vehicle, ft or in. (c = 72 in.)
C_D	drag coefficient, $C_D = \frac{D}{\frac{1}{2} \rho V^2 S}$
C_{D_o}	parasite drag coefficient
C_{D_m}	momentum drag coefficient
C_H	winglet hinge moment coefficient, $C_H = \frac{HM}{\frac{1}{2} \rho V^2 ce^2}$
C_L	lift coefficient, $C_L = \frac{L}{\frac{1}{2} \rho V^2 S}$
C_M	pitching moment coefficient, referenced to 50 percent chord unless noted by subscript, $C_M = \frac{M}{\frac{1}{2} \rho V^2 Sc}$
C_P	pressure coefficient, $C_P = \frac{p - p_o}{\frac{1}{2} \rho V^2}$
D	drag, lb
e	winglet effective span, in. (e = 2 in.)
f	number of weights forward (p. 45); (F-1) in Appendix A
F	ratio of local volume flux to exit volume flux, $F = \bar{A}\bar{U}$

h	height of vehicle above guideway, measured at 50-percent chord, ft or in.
$\bar{h}$	height of vehicle above guideway, measured at vehicle center of gravity, ft or in.
h_{TE}	height of vehicle trailing edge above guideway, ft or in.
HM	winglet hinge moment, referenced to winglet hinge axis, positive HM tends to increase gap, in.-lb.
$\Delta\bar{h}$	perturbation in height of vehicle above guideway measured at center of gravity of vehicle; vehicle moves away from guideway for positive $\Delta\bar{h}$, ft.
$I(\bar{\alpha})$, $I_M(\bar{\alpha})$	integrals defined by equations (A-15) and (A-21) respectively
I_w	winglet moment of inertia about winglet hinge axis, slug-ft^2
ℓ_w	winglet span measured from winglet axis of rotation, in. (ℓ_w = 1.5 in.)
L	lift, lb.
M	pitching moment, referenced to 50 percent chord, positive nose up, ft-lb
$\bar{M}$	Pitching moment, referenced to center of gravity of vehicle, positive nose up, ft-lb
p	local static pressure on bottom surface, psf
p_o	free-stream static pressure, psf
q	free-stream dynamic pressure, psf, $q = \frac{1}{2}\rho V^2$
r	dimensionless parameter, $r = \frac{2\delta}{W\alpha}$
r_N	r evaluated at $\bar{\alpha} = \bar{\alpha}_N$

Re	Reynolds number per foot, $Re = \frac{\rho V}{\mu}$
S	vehicle planform area including winglet area ($S = 6.75\ ft^2$)
U	local velocity, fps
U_E	exit velocity, fps
$\bar{U}$	dimensionless horizontal velocity, $\frac{U}{V}$
V	free-stream velocity, fps
w	velocity at side gap, normal to longitudinal axis of vehicle, fps
$\bar{w}$	dimensionless gap velocity, $\frac{w}{V}$
W	width of hull of vehicle, ft or in. ($W = 10.875$ in.)
W′	weight of vehicle, lb.
x	longitudinal location on model measured from leading edge, ft or in.
$\bar{x}$	non-dimensional longitudinal location, $\bar{x} = \frac{x}{c}$
$\bar{x}_{CP,\ LE}$	center-of-pressure location measured from leading edge
α	angle-of-attack of lower surface of vehicle, rad, $\alpha = 0.0377$ rad for $\theta = 0$
$\bar{\alpha}$	ratio of area change of lower surface from leading edge to trailing edge to exit area, $\bar{\alpha} = \frac{Wc\alpha}{A_E}$
$\bar{\alpha}_N$	$\bar{\alpha}$ for a height of winglet tip above guideway equal to 0.125 in. for a given θ_w
δ	winglet gap, distance from guideway lip to winglet tip, measured normal to guideway lip, ft

$\bar{\delta}$	ratio of gap to exit area $\bar{\delta} = \frac{2\delta c}{A_E}$
Δ	increment in variable
θ	pitch attitude of vehicle, rad or deg
θ_w	winglet rotation angle measured with respect to perpendicular to side of vehicle, rad or deg
λ	$\sqrt{\bar{A}^2 - 1}$
μ	viscosity of air, slugs per ft-sec
ξ	dummy integration variable, ft
ρ	density of air, slugs per ft^3
ϕ_G	angle of inclination of guideway lip, rad or deg
ω_N	natural frequency, Hz
$(\dot{})$	differentiation with respect to time.

Subscripts

$(\ )_{us}$	upper surface.
o	referenced to leading edge.

EXECUTIVE SUMMARY

This report is concerned with an examination of the aerodynamics of the tracked ram air cushion vehicle, a concept for high-speed ground transportation. Experimental and theoretical results are presented which relate to the aerodynamics associated with the longitudinal stability and ride qualities of this vehicle.

As the name implies, this vehicle is entirely supported by aerodynamic forces produced as a result of its forward speed. The concept is based on the nature of the forces produced by a wing operating very close to the ground; that is, high lift coefficients and high lift to induced drag ratios. Consequently, the aspect ratio of the wing can be reduced, resulting in hull shapes suitable for high-speed ground transportation vehicles. The lifting efficiency of the vehicle can be further improved by operating in a guideway and providing lateral seals with winglets mounted on each side of the hull. The aerodynamic interactions of the vehicle and guideway must be understood so that a configuration can be designed with high lifting efficiency, course stability, and satisfactory riding qualities. Ride quality and stability can be controlled by the basic shape of the vehicle, and in addition, by the flexibility of the winglets with respect to the hull. The objectives of this investigation have been to provide experimental data which will assist in understanding the vehicle/guideway interactions, and, to make it possible to estimate the longitudinal stability and ride quality.

Experimental results are presented from tests conducted on a model and section of guideway mounted in a wind tunnel and on the same model moving along a 300-foot guideway. Both wind tunnel and moving-model investigations were conducted since wind tunnel experiments on a vehicle operating very close to a fixed surface give rise to questions regarding the validity of the results due to the presence of the boundary layer on the guideway and the fact that the guideway is of finite length. Proper simulation of the aerodynamic boundary conditions can only be achieved with a moving model. Consequently, a series of moving-model experiments were conducted on a long guideway using a unique facility at Princeton University.

Extensive experimental data were taken in the wind tunnel related to the variation of lift, drag, and pitching moment with model height above the guideway and lateral gap. In addition, measurements were made of the winglet hinge moments and the pressure distribution on the guideway in the vicinity of the model. The moving-model experiments involved measurements of the equilibrium position of a towed model with respect to the guideway as a function of model weight and center-of-gravity position.

The experimental results indicate that high lift to induced drag ratios can be achieved. There is good agreement between the moving-model experiments and the wind tunnel experiments. The agreement is particularly good among the various stability derivatives or variations

in the forces and moments about equilibrium.

A theory for the longitudinal aerodynamic characteristics is developed and compared with the experimental results. The theory also agrees very well with the experimental results for these stability derivatives.

In summary, this report presents experimental data and theory for the longitudinal aerodynamic characteristics of a tracked ram air cushion vehicle which can be used to estimate the heave dynamics and ride quality with rigid and flexible winglets. Further experiments are planned to obtain additional information on the influence of pitch attitude on lift, drag, and pitching moment.

1. INTRODUCTION

One concept which appears particularly attractive for surface transportation at high speeds is the tracked ram air cushion vehicle. The lifting or supporting force for this vehicle is produced as a result of forward speed or what is referred to as the ram effect. No power source is directly used to develop lift at high speeds, that is, power is required for propulsion only, and the motion of the vehicle through the air produces lift. Versions of this vehicle have also been considered in which a part of the lifting force is produced by the propulsion system.(1)

The attractiveness of the concept, from an aerodynamic viewpoint, stems from two factors. First, very high lift to induced drag ratios can be achieved by a wing operating in close proximity to the ground.(2) Second, the presence of a guideway further increases the lifting efficiency by providing in effect, lateral seals or small gaps at the tips of the wings, essentially making the flow over the vehicle approximately two-dimensional and thus further improving the lift to induced drag ratio. Suitable combinations of these two effects make it possible to achieve high lift to induced drag ratios at the very low aspect ratios desirable for ground transportation vehicles.

The guideway or track serves two functions. In addition to providing lateral seals or small gaps to maintain nearly two-dimensional flow, a suitably shaped guideway can provide course stability such that the vehicle does not have to be continuously controllled, but rather is guided by the track as the name implies.

The configuration of the vehicle considered in this report is shown in Figure 1. The clearance between the trailing edge of the hull of the vehicle and the guideway is a comparatively large distance while the gap between the winglet tip and the guideway is comparatively small. As a consequence the ratio of these two dimensions is approximately 0.1 and therefore, variations in the winglet gap exert a much larger influence on the lifting force of the vehicle than do variations in the trailing edge height. This difference implies that the majority of the heave stiffness of the vehicle arises from the variation in the gap rather than the variation in the trailing edge height when the vehicle is displaced with respect to the guideway. It is therefore possible to alter significantly the heave stiffness and consequently the ride quality of the vehicle by providing winglet flexibility with respect to the hull, indicating the feasibility of varying the ride quality of the vehicle without the use of an active control system.

The object of the experimental investigation described in this report was to obtain quantitative data on the longitudinal aerodynamic characteristics (lift, drag, and pitching moment) of a typical tracked ram wing concept, to add to the studies reported in References 3 and 4. In particular, it was of interest to provide experimental data on the aerodynamics from which estimates of the ride quality and longitudinal dynamics can be made. Data are included which can be employed to predict the ride quality of the basic vehicle, as well as to examine the influence of winglet flexibility.

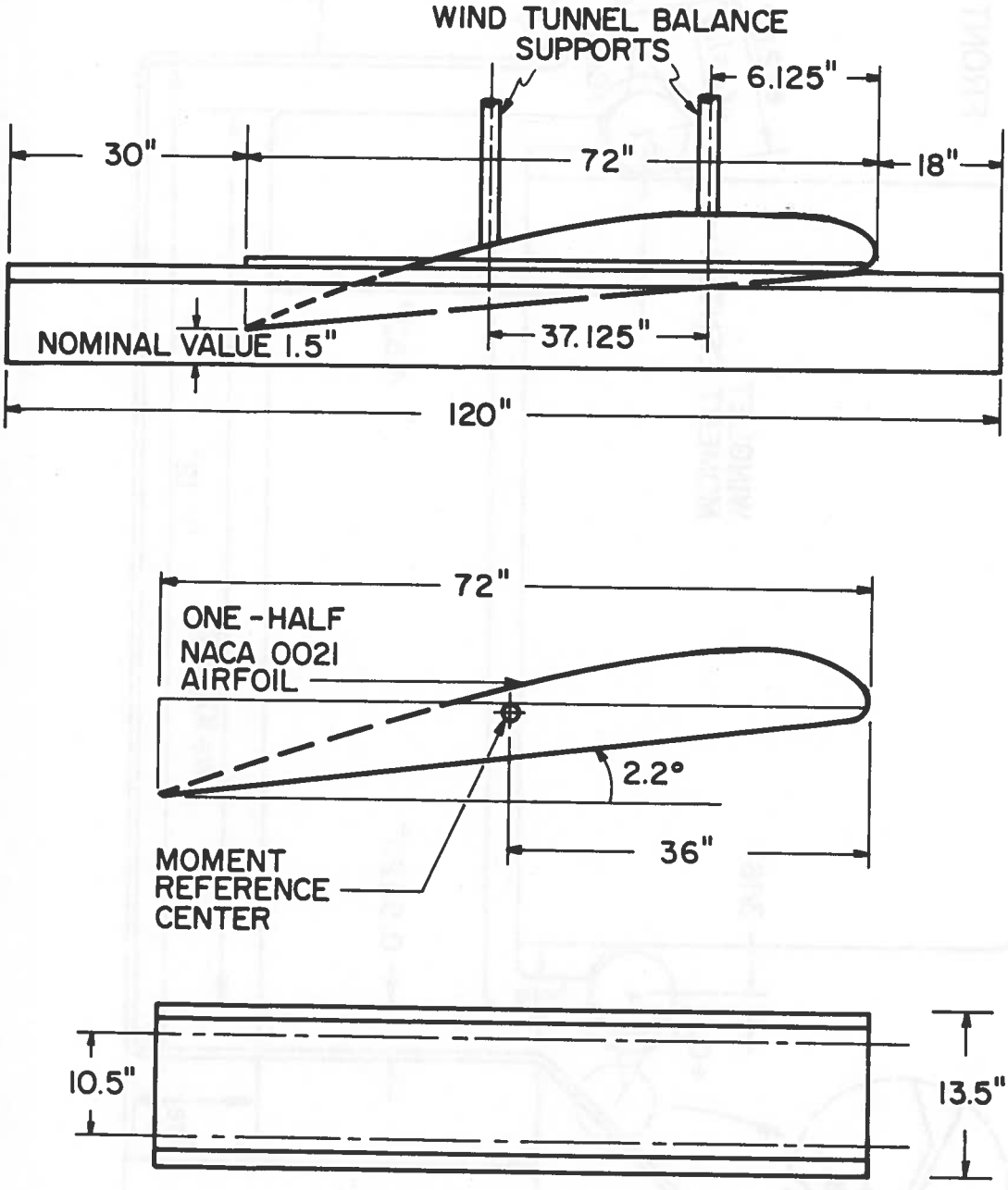

FIGURE 1. WIND TUNNEL MODEL CONFIGURATION.

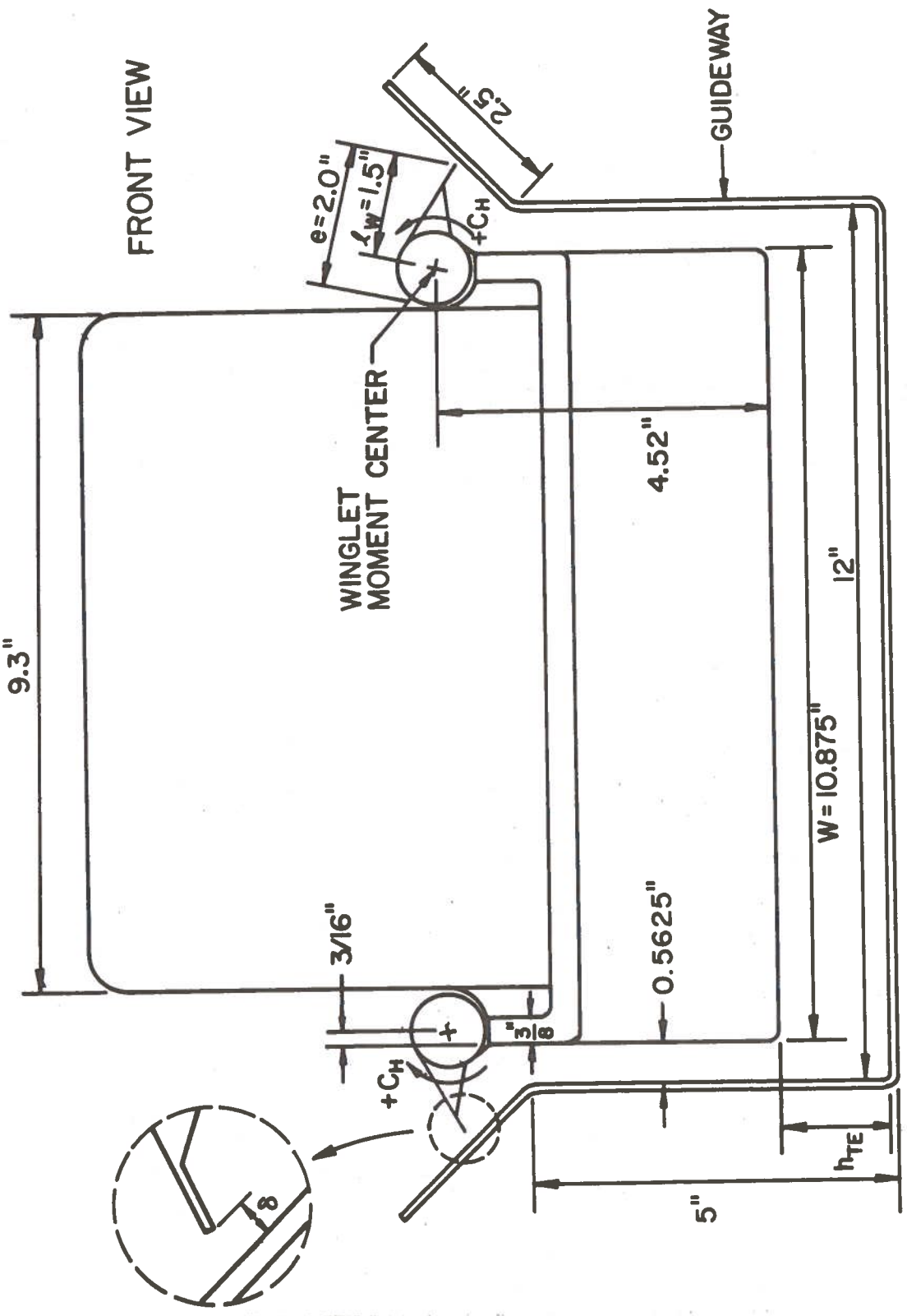

FIGURE 1. CONTINUED.

Two distinct sets of experiments are reported here. The first set was conducted in a wind tunnel. A section of the guideway and a model were mounted in a wind tunnel and a series of experiments were conducted to determine the variation in aerodynamic forces with various vehicle parameters. Direct measurements of the lift, drag, and pitching moment were made at various Reynolds numbers.

A second set of experiments involved the use of an identical model which was towed by a servo-controlled carriage along a 300-foot guideway. In the towed-model experiments, the model was essentially in free flight and lifting its own weight. The equilibrium position of the model with respect to the guideway was measured as a function of model weight and center-of-gravity position. From these equilibrium flight data it is possible to determine similar aerodynamic information to that measured in the wind tunnel tests. Difficulties were experienced with measurement of the drag force in the moving-model experiments and consequently drag data is not presented. The model attitude was not varied in the wind tunnel tests report so a complete comparison of the two sets of data is not possible, since the free flight experiments involve attitude variation. It is expected in the future to conduct experiments in the wind tunnel to measure attitude effects.

Each method has its advantages and disadvantages. In particular, the wind tunnel tests suffer from the disadvantage that there is a boundary layer present on the guideway which does not exist in the actual flight of the vehicle. The thickness of this boundary layer is an appreciable fraction of the distance between the model and the guideway

and may have a significant influence on the data. The boundary layer is of course not present in the moving-model experiments and therefore, better representation of the actual vehicle aerodynamics would be expected. One of the objectives of these experiments was to obtain an estimate of the importance of the presence of the boundary layer on the guideway.

Wind tunnel experiments tend to be somewhat more convenient with regard to studying large numbers of model parameter variations than the moving-model tests. Experience with these experiments however, showed this to be somewhat less true than was originally expected owing to the necessity of carefully setting and adjusting small clearances of the model with respect to the guideway in the wind tunnel tests.

Further, owing to limitations of the moving-model apparatus it is not possible to obtain as high a Reynolds number in the towed-model tests as can be achieved in the wind tunnel.

Thus, this report contains a description of the wind tunnel tests and a discussion of those results, a description of the towed-model tests and a discussion of those results and a comparison of these two sets of data where possible.

The towed-model configuration is geometrically identical to the wind tunnel model shown in Figure 1. The model employed in the wind tunnel tests had one variable geometric parameter. Each winglet could be rotated with respect to the body such that the gap between the winglet tip and the guideway could be varied independently of the height of the lower surface of the model above the guideway.

The lip of the guideway was selected to be an angle of 45 degrees from the vertical to provide lateral as well as longitudinal stability. A number of experiments with a free-flight powered model as well as the towed-model experiments described here, indicated that this guideway configuration results in a vehicle which is stable both longitudinally and laterally. The influence of the guideway lip angle can be seen by examining the effects of motion of the vehicle in the guideway on winglet gap. Changes in the winglet gap produce the primary changes in lower surface pressure since the gap is a much smaller dimension (the order of 0.1 in) than the height of the trailing edge above the guideway (the order of 1.5 in). Basically, as may be seen in the sketch in Figure 2, vertical guideway lips would provide a strong lateral restoring force with lateral displacement owing to the fact that the change in gap would be equal to the lateral displacement of the model. The vertical restoring force variation with height would be small since height changes would produce no change in gap. In the case of horizontal guideway lips, just the opposite would be true, a strong vertical force variation with height would be expected and only a small lateral force variation with lateral displacement would be expected. As a compromise between these two limits therefore, the 45 degree angle was chosen. For simplicity, the bottom surface of the model had a constant slope, and the configuration in no sense represents an optimized design.

A free-flight powered model, which was employed for some qualitative experiments, did in fact obtain some additional lift augmentation from a ducted fan propulsion system similar to the configuration

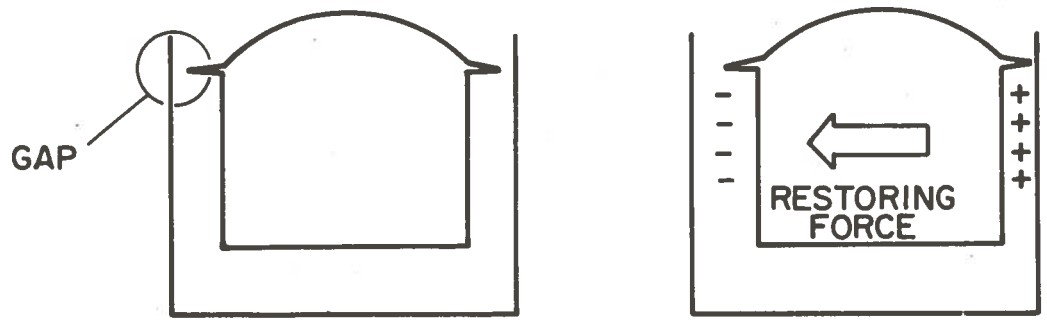

VERTICAL GUIDEWAY LIPS PRODUCE LATERAL RESTORING FORCE

VERTICAL MOTION PRODUCES NO GAP CHANGE

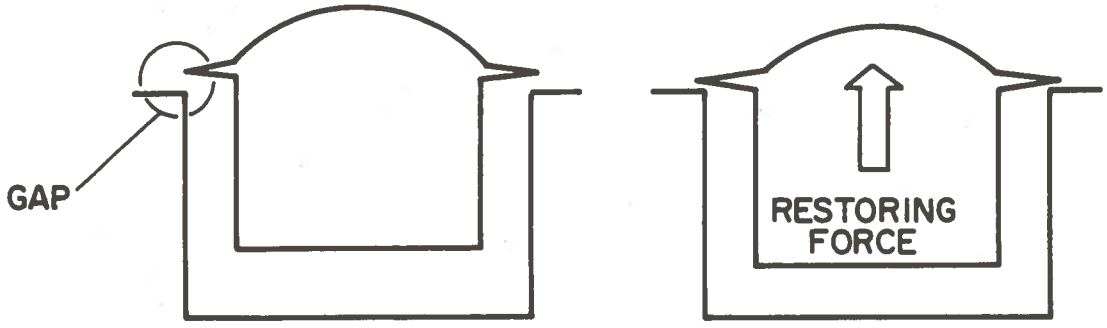

HORIZONTAL GUIDEWAY LIPS PRODUCE STRONG VERTICAL RESTORING FORCE

HORIZONTAL MOTION PRODUCES NO GAP CHANGE

FIGURE 2. INFLUENCE OF GUIDEWAY GEOMETRY ON RESTORING FORCE.

described in Reference 1. The models employed in the wind tunnel and towed tests did not incorporate a propulsion system since the interest in the experiments centered around the aerodynamics of the basic configuration.

A brief series of experiments were conducted to evaluate the dynamics of the free winglets. The results are presented and discussed. Interest in the free winglet case was related to the fact that one way of controlling the vertical ride quality of this vehicle is to provide spring restrained winglets. Data are presented for winglet natural frequency and damping.

Appendix A describes a theory to predict the pressure distribution on the bottom surface of the vehicle. Expressions are given for the lift and pitching moment coefficients produced by the bottom surface pressure. Theoretical predictions are compared with the wind tunnel and towed-model experimental results.

2. DESCRIPTION OF MODEL AND APPARATUS

2.1 MODEL

Drawings showing the model and guideway geometry are presented in Figure 1.

The lower surface of the model is flat with a slope of approximately 2.2 degrees. The upper surface of the model is one-half of an NACA 0021 airfoil. The winglet cross section consisted of a tube with a fairing as shown in Figure 1. The model was constructed so that the winglets could be independently rotated with respect to the body and locked in any desired position to alter the relationship between the side gap and the bottom height. Alternatively the winglet could be spring restrained such that its free dynamic motion could be examined. The towed model and the wind tunnel model were geometrically identical but fabricated from different materials. In order to reduce the weight of the towed model, its basic hull was constructed of balsa wood. The wind tunnel model hull was constructed of aluminum to withstand higher dynamic pressures.

The winglets on the wind tunnel model were constructed of balsa wood and fiberglass attached to a thin-walled aluminum tube. The towed-model winglets were constructed entirely of balsa wood. The straightness of the winglet tip and therefore, a measure of the gap variation over the length of the model was ±0.015 in. A seal was provided between the winglet and the hull of the model. The same upper surface was employed on both models. The upper surface, one-half of an airfoil section, was

constructed of styrofoam and covered with doped tissue to provide a smooth finish.

Strain gage instrumentation in the interior of the model was provided to measure the winglet hinge moment as shown in Figure 3.

The guideway sections were fabricated from sheet steel. The section employed in the wind tunnel was identical in cross section to the 300-foot section constructed for the towed-model tests but was of heavier gage steel. Figure 1 shows the cross section of the guideway installed in the wind tunnel as well as the cross section of the guideway employed with the towed model.

The wind tunnel model was attached to the wind tunnel balance by two struts. The model and guideway were mounted inverted to provide access to the balance, as well as to eliminate the necessity of having the support struts pass through the guideway, as shown in Figure 4.

The geometry for the towed-model tests is shown in Figure 5 and the complete installation is shown in Figure 6.

2.2. APPARATUS, INSTRUMENTATION, AND TEST PROCEDURE

2.2.1. Wind Tunnel Tests

The wind tunnel tests were conducted in the Princeton University Subsonic Wind Tunnel. The test section measures four feet by five feet. The tunnel is a closed circuit type, capable of airspeeds up to 150 fps. It is equipped with a direct readout six component pneumatic balance. As mentioned above the winglets were provided with strain gages for measurement of winglet hinge moments. In addition, 67 pressure taps

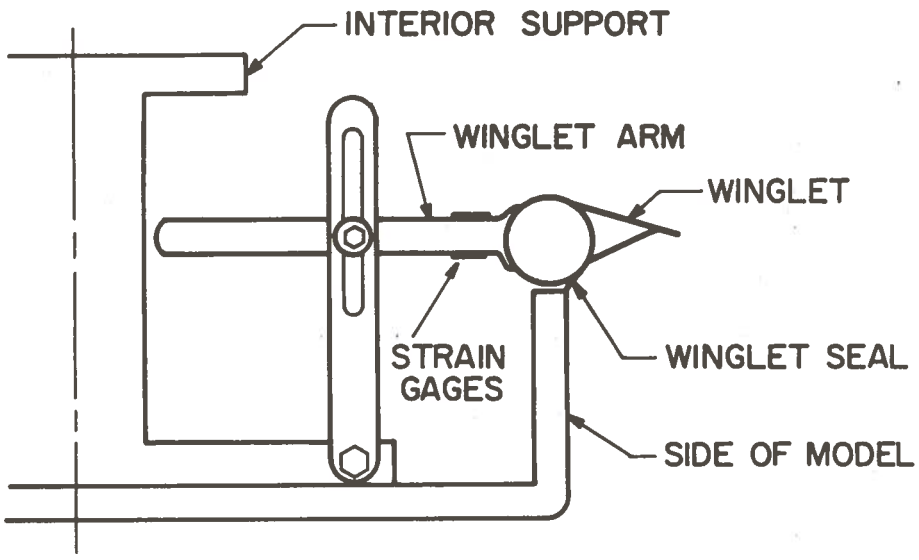

WINGLET-FIXED CONFIGURATION

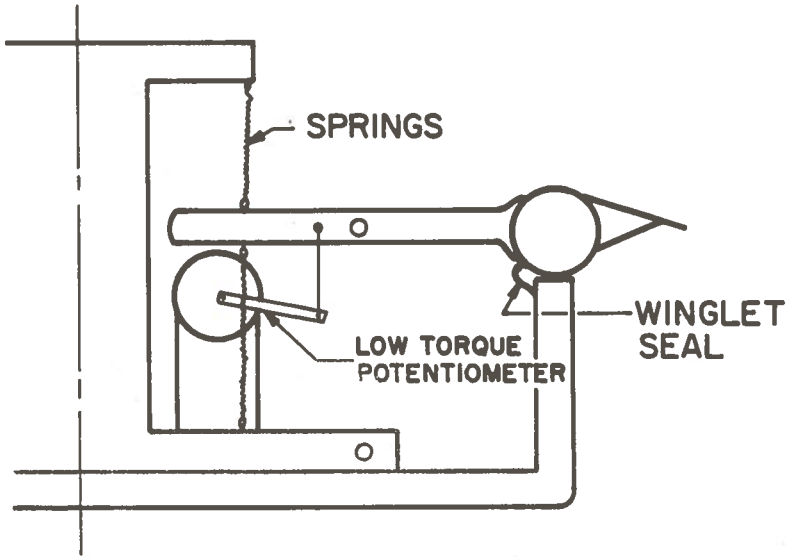

WINGLET-FREE CONFIGURATION

FIGURE 3. WINGLET MOUNTING AND INSTRUMENTATION.

FIGURE 4. MODEL INSTALLED IN WIND TUNNEL.

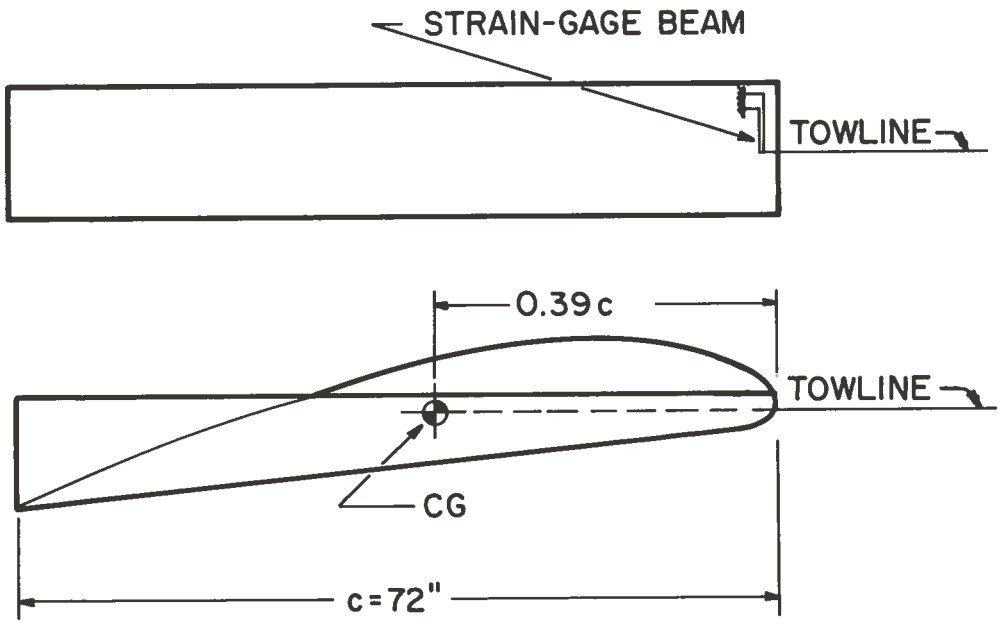

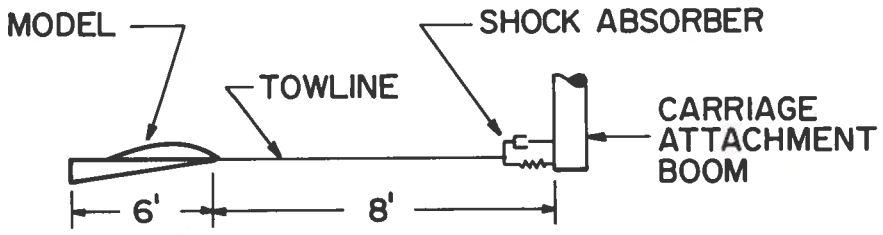

FIGURE 5. TOWED-MODEL CONFIGURATION.

FIGURE 6. TOWED MODEL AND APPARATUS.

were located at various stations on the guideway, as shown in Figure 7, to provide data on the distribution of the aerodynamic force acting on the vehicle.

Considerable care was required in setting up the wind tunnel model for various experiments owing to the small clearances involved.

A variety of winglet positions and trailing edge heights relative to the guideway were examined at various wind tunnel velocities. The geometric variables of the wind tunnel tests are listed in Table I. Four free-stream velocities were examined to evaluate the influence of Reynolds number on forces and moments and pressure distributions.

Repeat of a considerable number of the wind tunnel tests was required. A strong dependence of the force and moment coefficients on free-stream velocity was noted during the initial experiments. This was found to be a result of airflow from the interior of the model exiting at the juncture between the model support strut and the upper surface of the model producing a strong cross flow and resulting in significant separation on the upper surface of the model. The strut support was redesigned to provide a seal in this area reducing markedly the variation of the coefficients with tunnel dynamic pressure. The experimental data from the wind tunnel are presented for one dynamic pressure (10.4 psf). Less than 5 percent variation of the coefficients from values at this dynamic pressure was noted over the range from 5 to 20 psf. Some of this variation is a result of small deflections of the model with respect to the guideway which will be treated fully in a later report.

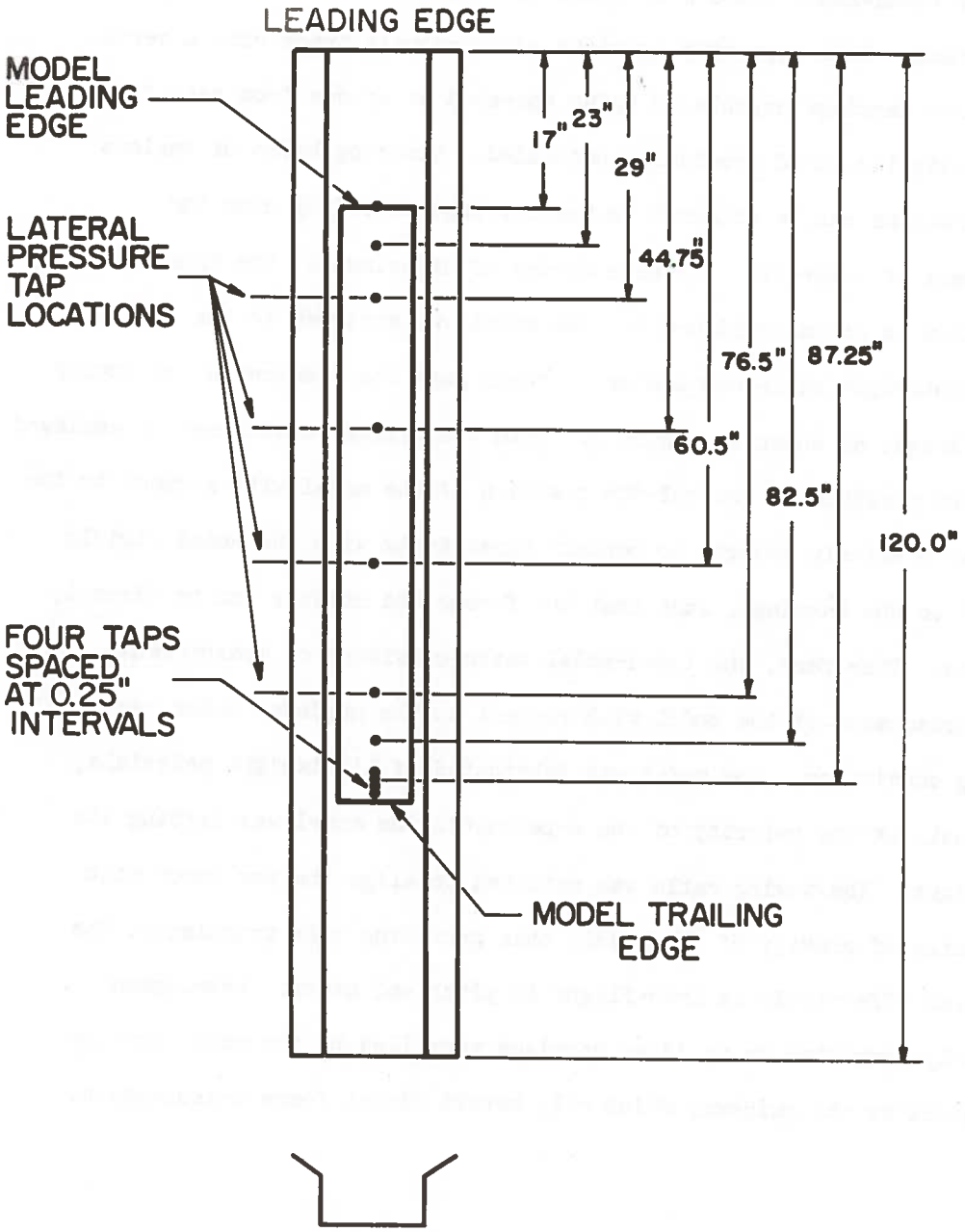

FIGURE 7. GUIDEWAY PRESSURE TAP LOCATIONS, WIND TUNNEL.

2.2.2. Free-Flight Towed-Model Tests

The towed-model tests were conducted using the Princeton Dynamic Model Track. This apparatus consists of a monorail track with a servo-controlled carriage capable of being operated at speeds from zero to 40 fps with its speed precisely controlled. Mounting booms of various configurations can be attached to the carriage depending upon the experiment of interest. In these series of experiments, the boom configuration is shown in Figure 6. The model was attached to the carriage by a lightweight cable containing a strain gage for measurement of towing force (drag), as shown in Figure 5. With the carrage configuration employed it is not possible to control the position of the model with respect to the guideway precisely enought to conduct these tests with the model rigidly mounted to the carriage, such that the forces and moments can be directly measured. Therefore, the towed-model tests consisted of measurements of the displacement of the model with respect to the guideway under various loading conditions. The model was fabricated of lightweight materials, such that, at the velocity of the experiments the model was lifting its own weight. The towing cable was attached to align the tow force with the center of gravity of the model, thus providing only propulsion. The model was effectively in free-flight in pitch and heave. Development is nearly completed on an idler carriage propelled by the main carriage but guided by the guideway which will permit direct force measurements.

Owing to cost considerations, the guideway installed did not run the full length of the Dynamic Model Track, and therefore, a rather elaborate injection and removal device was developed to place the model precisely in the guideway and remove it smoothly and without damage at 35 to 40 fps model speed. This device is shown in Figure 8. For further experiments it appears highly desirable to extend the length of the guideway to simplify testing and eliminate the need for this injection system.

The guideway has adjustment supports located every five feet to control its geometry. A transit was used to survey the guideway periodically to insure straightness of the guideway during the experiments.

The model was brought up to speed mounted on a small carriage and guided by a wire under high tension to the entrance of the guideway. The small carriage was separated from the model at the entrance of the guideway and the model proceeded down the guideway towed at the desired speed at a height and attitude with respect to the guideway, determined by the loading condition of the model and the aerodynamic forces acting on the model. Since the longitudinal motion of the model was stable it would, within a short time after entering the guideway, take up a stable equilibrium condition and maintain this condition until it left the guideway. During the course of this steady-state condition, measurements of the equilibrium height and attitude of the model were made.

The servo-controlled carriage contains power supplies to power the model instrumentation as well as a 43 channel telemeter system which transmits measured data from the moving model to a nearby ground

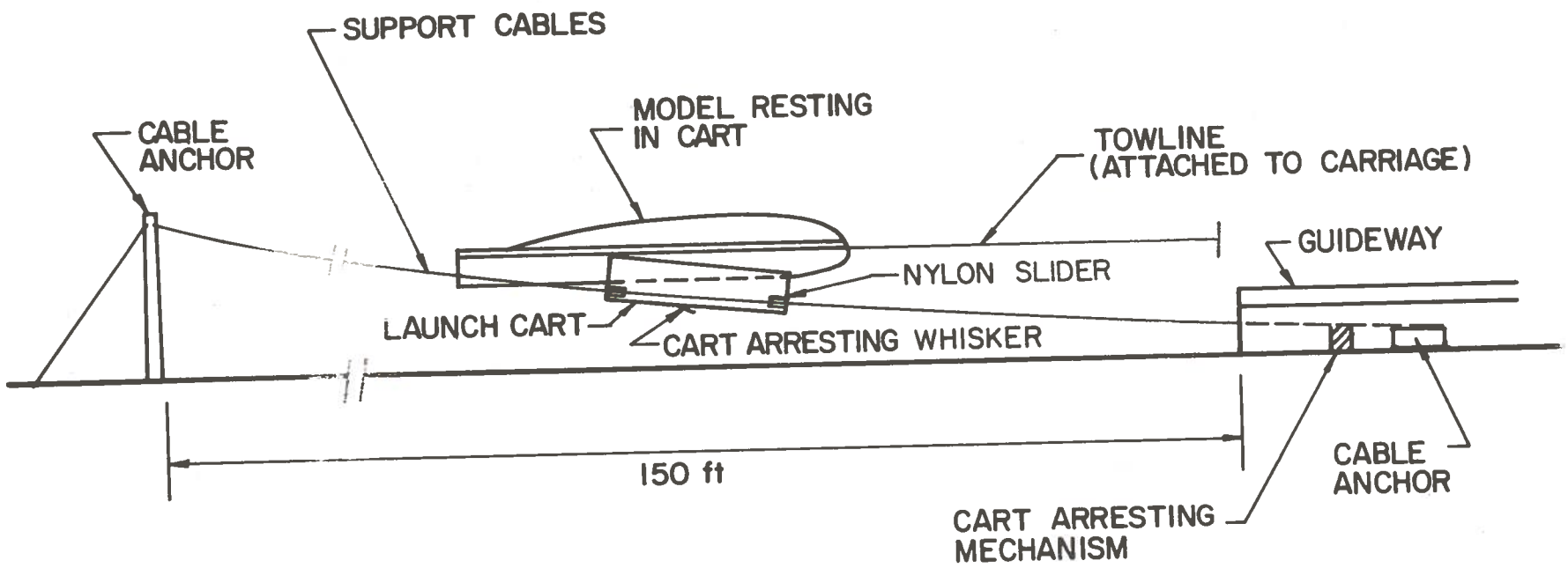

FIGURE 8. GUIDEWAY INJECTION SYSTEM, TOWED MODEL.

station.

In addition to the towing force or drag of the model and the carriage speed, measurements of the height of each of the outer corners of the winglets above the guideway were made. These measurements were made with low friction potentiometers mounted in the four locations, each sensing the height of one corner of the model. Analog circuitry was then used to sum and difference these four individual measurements such that the average height of the winglets above the guideway and the model pitch attitude could be directly read. The location and geometry of these sensors is shown in Figure 9. Tow force data are not presented here owing to the absence of information on the drag of the height-sensing whiskers.

The winglet hinge moments were not measured in this series of experiments owing to the necessity of providing additional winglet supports to prevent torsional deflections of the balsa wood winglets. Due to an experimental error, preliminary indications from the wind tunnel data were that the center of gravity of the towed model would have to be located near the 25 percent chord point to achieve pitching moment equilibrium with a level attitude. This design constraint made it impossible to employ the winglets used in the wind tunnel tests as they would have comprised most of the weight of the towed model and as a consequence, the center of gravity of the free flight model would have been located in the vicinity of 40 to 50 percent chord. Consequently, lightweight winglets were constructed so that the center of gravity could be moved forward to a position required for level attitude equilibrium. However, later corrections to the wind tunnel tests

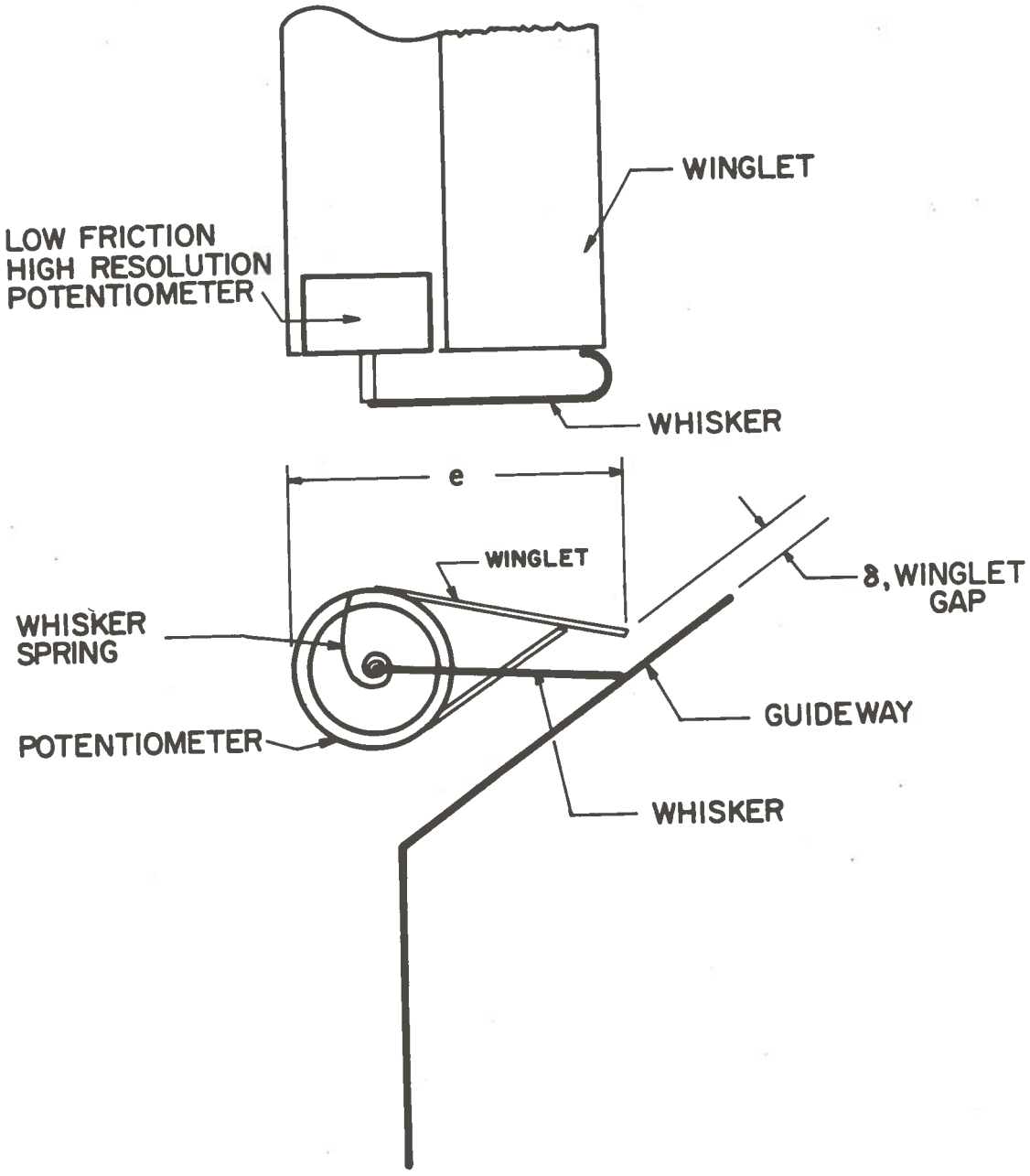

FIGURE 9. DISPLACEMENT MEASURING SYSTEM, TOWED MODEL.

indicated that a more aft center of gravity, as would have been obtained with the heavier winglets, would have produced satisfactory equilibrium. The towed-model tests confirmed the aft location of the center of pressure.

3. DESCRIPTION OF TESTS

3.1 WIND TUNNEL TESTS

The wind tunnel tests were all performed with the model in a level attitude with respect to the guideway. That is, the winglet tips were parallel to the guideway lip in the longitudinal direction. Two values of the clearance between the trailing edge of the model and the bottom surface of the guideway, 1.28 and 1.44 in. were examined, and the winglet/guideway clearance was varied from 0.050 in. to 0.150 in. Table I lists the model test conditions. The tests were conducted by adjusting the trailing edge height to a selected value and then rotating the winglet to obtain various values of the winglet/guideway gap.

In order to examine the influence of Reynolds number the tunnel dynamic pressure was varied from 5.2 to 20.8 psf as indicated in Table I. The Reynolds number per foot corresponding to each of these velocities is also given in the table. In addition, the displacement thickness of the boundary layer at the trailing edge of the vehicle is indicated in this table to give some estimate of the possible importance of the boundary layer. This thickness is based on flat plate theory assuming transition occurs at $Re = 5 \times 10^6$.

Extensive preliminary runs were made to establish the repeatability of the data. The balance readings and pressure distributions were typically repeatable to ± 3 percent. Some initial wind tunnel experiments were conducted at a dynamic pressure of 1.37 psf, similar to that of the

TABLE I WIND TUNNEL TEST CONDITIONS

a. Dynamic Pressure, Reynolds Number, and Estimated Boundary Layer Thickness

Velocity fps	Nominal Dynamic Pressure psf	Nominal Reynolds No. per ft.	Boundary Layer Displacement* Thickness at Trailing Edge in.
66	5.2	4.2×10^5	0.19
92	10.4	5.9×10^5	0.18
114	15.6	7.3×10^5	0.18
132	20.8	8.4×10^5	0.18

*Transition assumed to take place at $Re_x = 5 \times 10^5$.

b. Dimensional Location of Model with Respect to Guideway and Corresponding Dimensionless Parameters

Winglet Gap δ in.	$r = \frac{2\delta}{W\alpha}$
0.050	0.24
0.075	0.36
0.100	0.49
0.125	0.60
0.150	0.73

Trailing Edge Height h_{TE} in.	$\bar{\alpha} = \frac{W_c \alpha}{A_E}$
1.28	1.39
1.44	1.31

towed-model tests. Although tests at this dynamic pressure gave results which were close to those at higher dynamic pressures, difficulties were experienced with the sensitivity of the wind tunnel balance as a result of the small forces produced and so these data are not presented, Pressure distributions were made manually and the manometer board was tilted to 45 degrees to obtain suitable sensitivity.

Variations in the coefficients with tunnel velocity existed in the results although the variations were typically less than 5 percent of the results presented. These variations may arise from one or more of several sources; the influence of Reynolds number, static deflection of the model owing to wind tunnel balance compliance, winglet elastic deflections, upper surface aerodynamic effects or tunnel floor interference effects. The importance of the deflection of the model with respect to the guideway will be discussed more completely in a later report. This report will include the effects of pitch attitude variation. This data is necessary to interpret the effect of model deflection.

Tuft studies were made of the flow over the upper surface of the model to determine if any separated flow was present. Generally the flow was attached over the majority of the upper surface at all velocities. A small leading edge separation bubble was detected at 34 fps. The bubble disappeared at higher velocities and very little trailing edge separation was detected. A leading edge trip wire was installed and found to have no measurable influence on the force and moment measurements. Some experiments were also conducted with the rear portion of the upper surface fairing removed. This modification also had no noticeable influence on the variation of the force coefficients with velocity so that Reynolds number effects do

not appear to be a significant factor.

3.2 TOWED-MODEL TESTS

The towed-model tests were all conducted at a velocity close to 34 fps. It was initially expected that wind tunnel tests could be conducted at this same velocity such that both series of tests would be conducted at the same Reynolds number. However, as mentioned above, the sensitivity of the wind tunnel balance was not sufficient to conduct wind tunnel tests at this low dynamic pressure. The weight of the model with no ballast was 3.78 lb and weights were added in unit increments of 0.214 lb to produce various lift coefficients and center of gravity positions for the experiments. The center of gravity of the model with no ballast was at 39 percent chord.

The velocity of the model was measured by a tachometer installed on the carriage as well as by precision clocks stationed at 25 foot intervals along the track.

At three winglet rotation angles, a series of runs at nominally constant velocity were made with various ballast locations, to produce different equilibrium lift coefficients and center-of-gravity positions. The height of each corner of the model was measured continuously as a function of time during each run. Portions of each run, for which the time histories of the model position, with respect to the guideway, showed that the model was in a steady-state condition, were selected and analyzed to determine the equilibrium position of the model.

In the majority of the test conditions, no difficulty was experienced

in achieving a sufficiently long steady-state portion during a run. In some cases, at the maximum winglet/guideway gaps examined, the model had a tendency to exhibit a lightly damped long period oscillation, making it difficult to determine the steady-state condition, and producing scatter in the measured equilibrium conditions.

4. DISCUSSION

4.1 WIND TUNNEL DATA

4.1.1 Force and Moment Data

The lift coefficient, drag coefficient, and pitching moment coefficient referred to the 50 percent chord station where measured as a function of two non-dimensional parameters, r, a non-dimensional measure of the winglet gap, with respect to the guideway, and $\bar{\alpha}$, a non-dimensional measure of the height of the trailing edge of the vehicle above the guideway.

The various coefficients varied less than 5 percent over the range of tunnel dynamic pressures indicated in Table I. The variations of the lift, drag, and pitching moment coefficients with the most significant parameter, r, were found to be essentially independent of dynamic pressure. It is these variations that are of greatest importance in determining the stability and ride quality. Therefore, only the results obtained at an intermediate dynamic pressure of 10.4 psf are presented and discussed in some detail as representative of the aerodynamics of the vehicle.

Figure 10 shows the experimental results for the variation of the aerodynamic coefficients with the parameters, r and $\bar{\alpha}$.

The contribution of variations in r and $\bar{\alpha}$ to the variation in the coefficients of a rigid vehicle in heave can be evaluated by examining the change in a coefficient with vehicle height in terms of variations with r and $\bar{\alpha}$ as

$$\frac{d(\ )}{d(\Delta h)} = \frac{d(\ )}{dr}\frac{dr}{d(\Delta h)} + \frac{d(\ )}{d\,\bar{\alpha}}\frac{d\,\bar{\alpha}}{d(\Delta h)},$$

where for a rigid vehicle, i.e., winglets fixed with respect to the body

$$\Delta\delta = \frac{\Delta h}{\cos \phi_G} \quad \text{and} \quad \Delta A_E = W\,\Delta h,$$

so that introducing the definitions of r and $\bar{\alpha}$

$$\frac{W\alpha}{2}\frac{d(\ )}{d(\Delta h)} = \cos \phi_G \frac{d(\ )}{dr} - \frac{\bar{\alpha}W}{2c}\frac{d(\ )}{d\,\bar{\alpha}}.$$

The vehicle of interest here has a low aspect ratio such that, $\frac{W}{c} = 0.15$. Consider the lift coefficient variation as an example. It can be seen from Figure 10 that the dimensionless variation of the lift coefficient with $\bar{\alpha}$ is a similar magnitude or somewhat smaller than its variation with r, and as a consequence, the above expression indicates that the major contribution to the heave aerodynamics arises from the first term and the second term contributes from 5 to 10 percent of the total. This result also indicates that it is possible to obtain significant variations in the heave dynamics of the vehicle by allowing the winglets to move with respect to the body so that the parameters r and $\bar{\alpha}$ may vary independently. The basic data with $\bar{\alpha}$ and r as independent parameters can be used to

estimate the winglet-free dynamics.

The experimental data presented in Figure 10 indicate the following trends. The lift coefficient decreases with increasing gap height and also with increasing trailing edge height (decreasing $\bar{\alpha}$). The drag coefficient increases with increasing gap and also with increases in trailing edge height (decreasing $\bar{\alpha}$). Both of these trends are physically reasonable indicating the favorable effects on lift and drag of operating an aerodynamically supported vehicle in close proximity to the ground. The dependence of the lift/drag ratio on r and $\bar{\alpha}$ is shown in Figure 11. A maximum lift/drag ratio of 36 was measured at the lowest trailing edge height and minimum gap. Again, this very high lift/drag ratio indicates the favorable effect of operating an aerodynamically supported vehicle very close to the ground.

The pitching moment coefficient, referenced to the 50 percent chord point, also shown in Figure 10, decreases with increasing winglet gap and shows only a weak dependence on trailing edge height. Note that the presence of this variation implies that the dynamic motions in heave and pitch are coupled. That a change in height of the vehicle will produce a change in the pitching moment which will result in an angular acceleration and consequently an attitude change. The center-of-pressure location is shown in Figure 11, referenced to the leading edge of the model. The center of pressure is located about 39 percent chord aft of the leading edge of the model and appears to be almost independent of the winglet gap and the

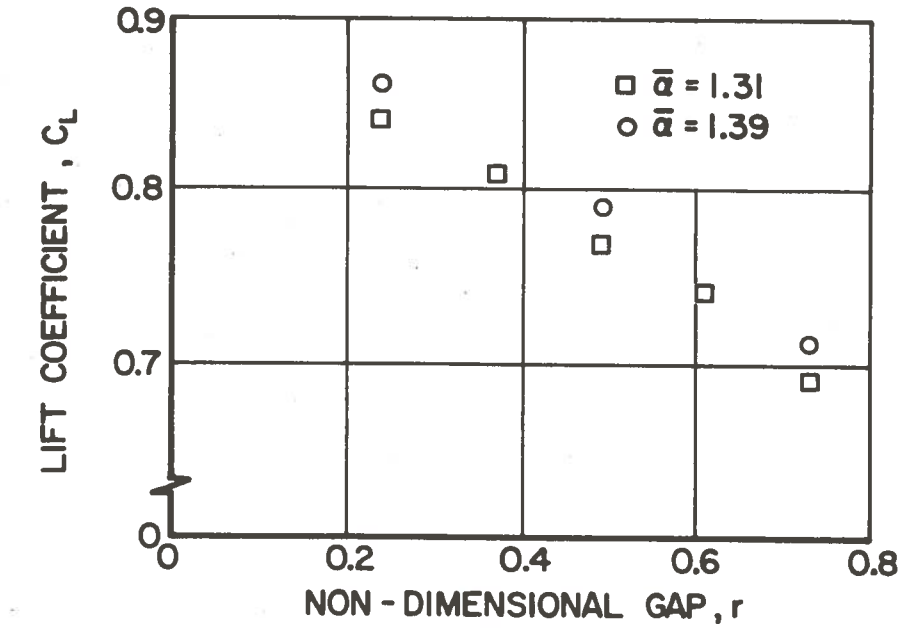

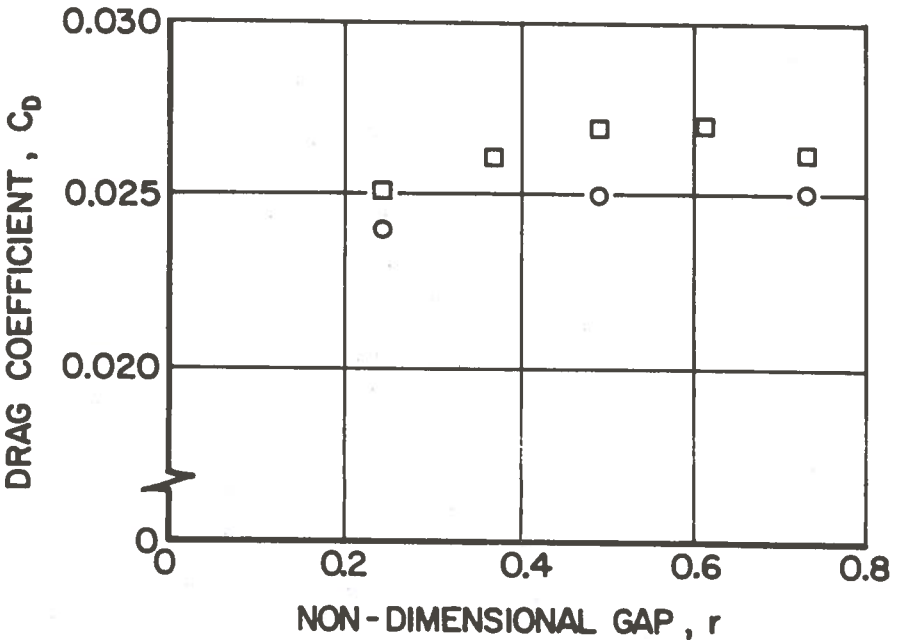

FIGURE 10. WIND TUNNEL DATA.

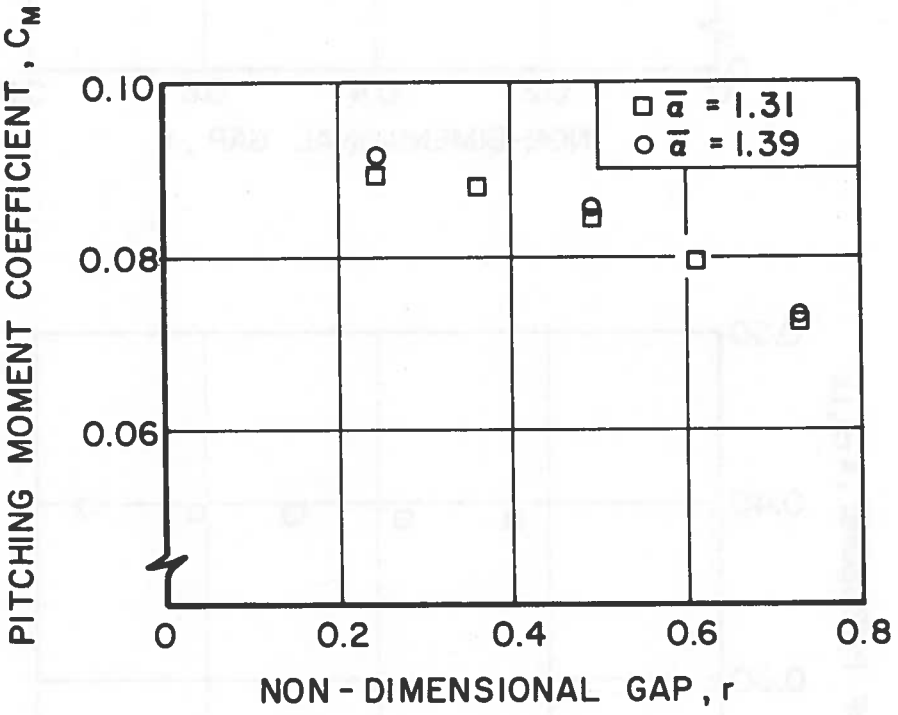

FIGURE 10. CONTINUED.

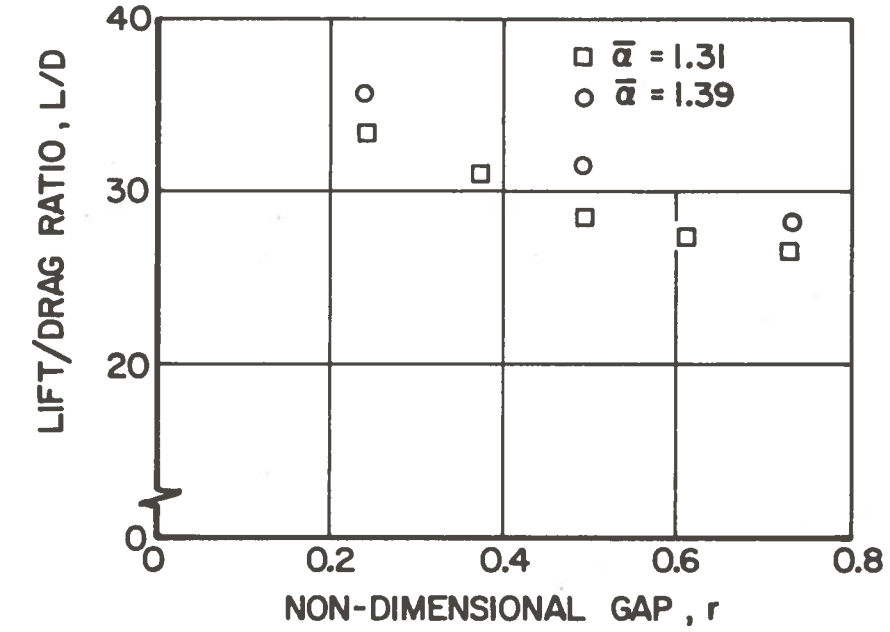

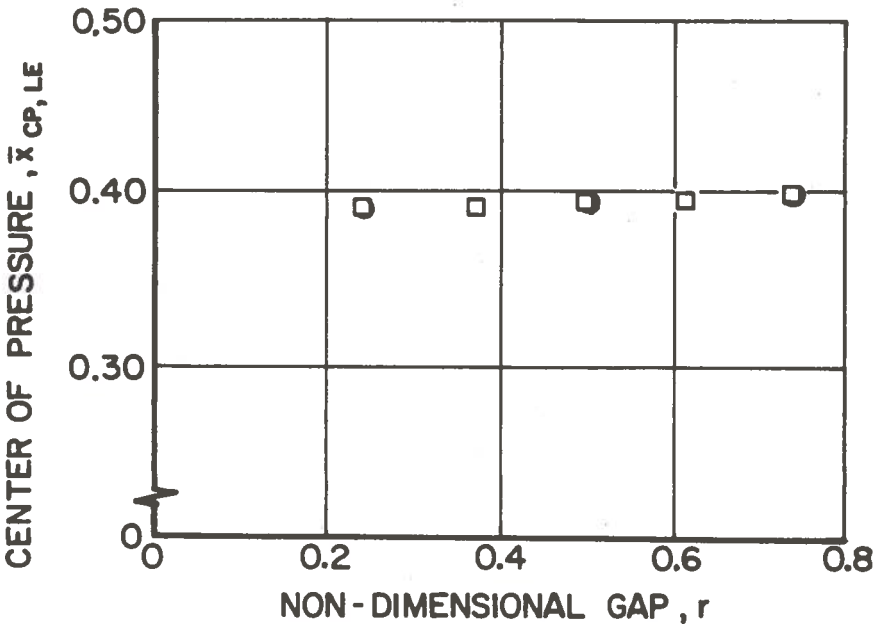

FIGURE 11. LIFT/DRAG RATIO AND CENTER OF PRESSURE, WIND TUNNEL DATA.

trailing edge height. This result indicates that the heave and attitude motions of the vehicle would be relatively uncoupled if the vehicle center of gravity were located at this longitudinal position.

4.1.2 Pressure Distribution Data

In addition to force and moment data, pressure distribution measurements were made using static pressure ports located on the guideway. Pressure distributions along the longitudinal centerline of the guideway are shown in Figure 12a. They indicate the general shape of the pressure distribution expected from the theory described in Appendix A with the exception that the pressure coefficient is slightly negative at the trailing edge. Spanwise pressure distributions were also measured and a typical result is shown in Figure 12b, indicating that the pressure is approximately constant in the spanwise direction across the guideway. Near the winglet lip the pressure rapidly decreases. The pressure decrease occurs farther inboard as the gap is increased.

4.1.3 Winglet Data

The winglet hinge moment was also measured. The hinge moment coefficient is referenced to the winglet area and winglet span and is measured about the axis of the winglet. The results presented in Figure 13 indicated that the center of pressure is roughly 25 percent of the span of the winglet outboard of the hinge axis. The hinge moment variation with trailing edge height appears to be somewhat opposite from what one would expect on the basis of the lift coefficient variation. That is, since it is approximately true

that the primary source of the lift is the pressure distribution on the lower surface of the vehicle and it would be expected that this pressure is reflected on the lower surface of the winglet, one would expect that the winglet hinge moment would be largest at the lowest trailing edge height. The data indicate just the opposite trend, perhaps reflecting some of the complexities in the flow field as a result of the nozzle effect at the exit.

In addition to these hinge moment data, experiments were performed in the wind tunnel to measure the winglet-free dynamics. In these experiments, one winglet was allowed to rotate about its hinge line and was restrained by mechanical springs as shown in Figure 3. Also experiments were conducted without the spring restraint, but with the winglet center of gravity located to balance the steady aerodynamic hinge moments. In both experiments the equilibrium winglet gap was maintained at 0.125 in. ($r = 0.61$) by adjusting the spring or mass preload for each dynamic pressure.

The results of these experiments are presented in Figures 14 and 15 which show the free-winglet frequency and damping factor as functions of free-stream dynamic pressure. In Figure 14 the low-frequency measurements show excellent agreement with the undamped natural frequency of the winglet motion predicted by the static measurements of winglet hinge moments presented in Figure 13, combined with the measured winglet inertial characteristics. This agreement indicates that in this frequency range unsteady effects are not important and static hinge moment data are acceptable for

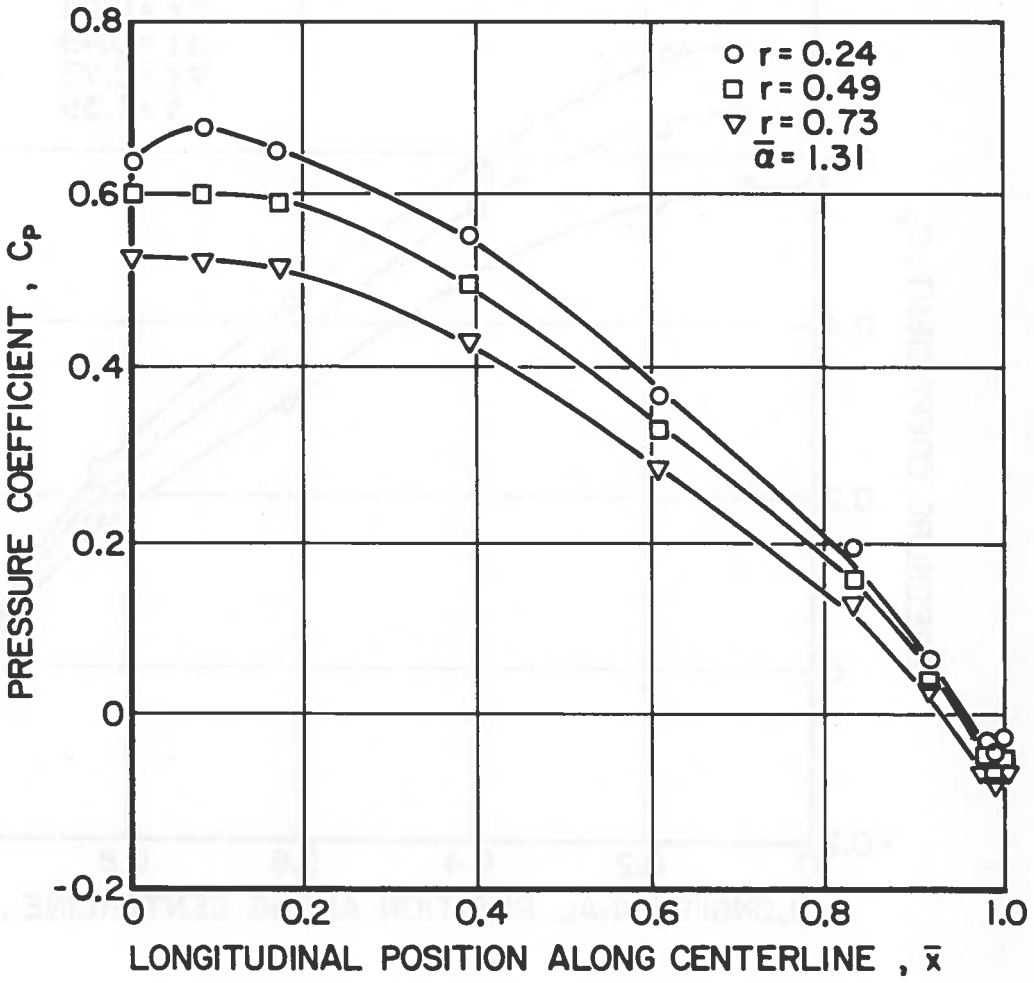

FIGURE 12a. LONGITUDINAL PRESSURE DISTRIBUTION, WIND TUNNEL DATA.

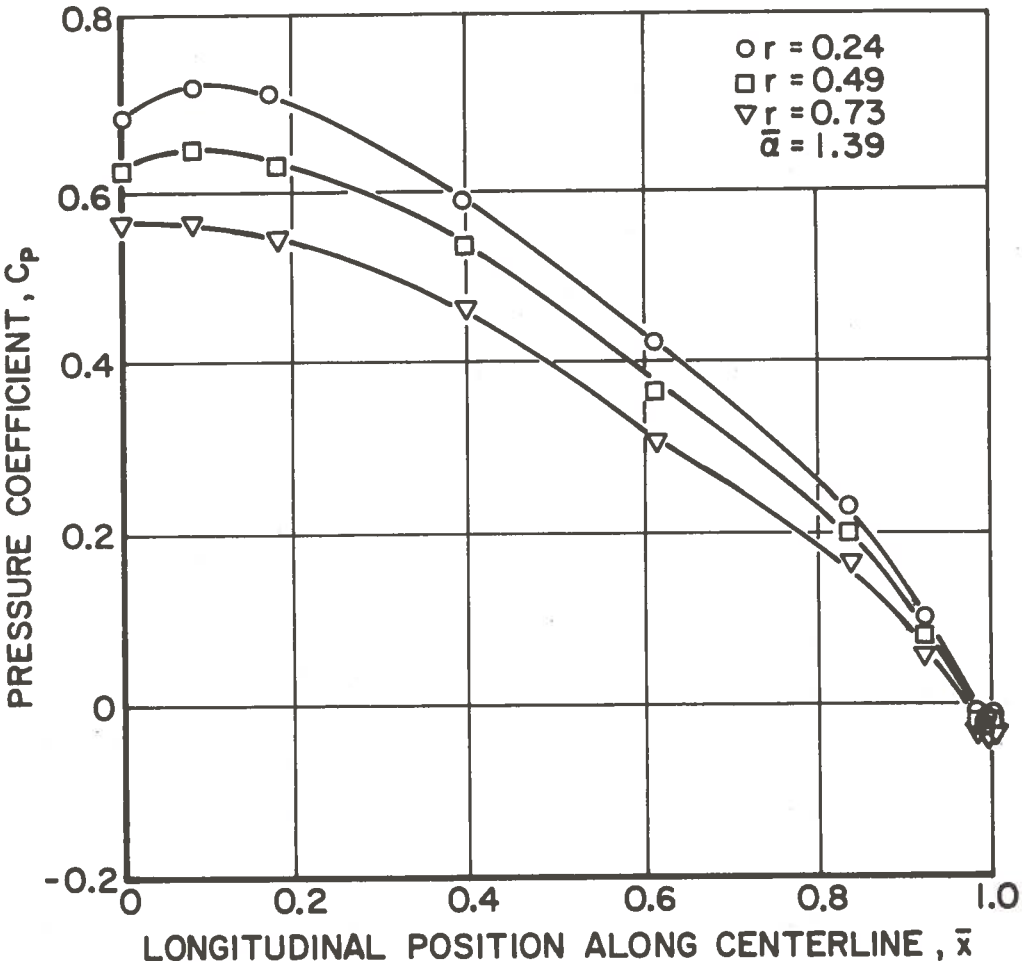

FIGURE 12a. CONTINUED.

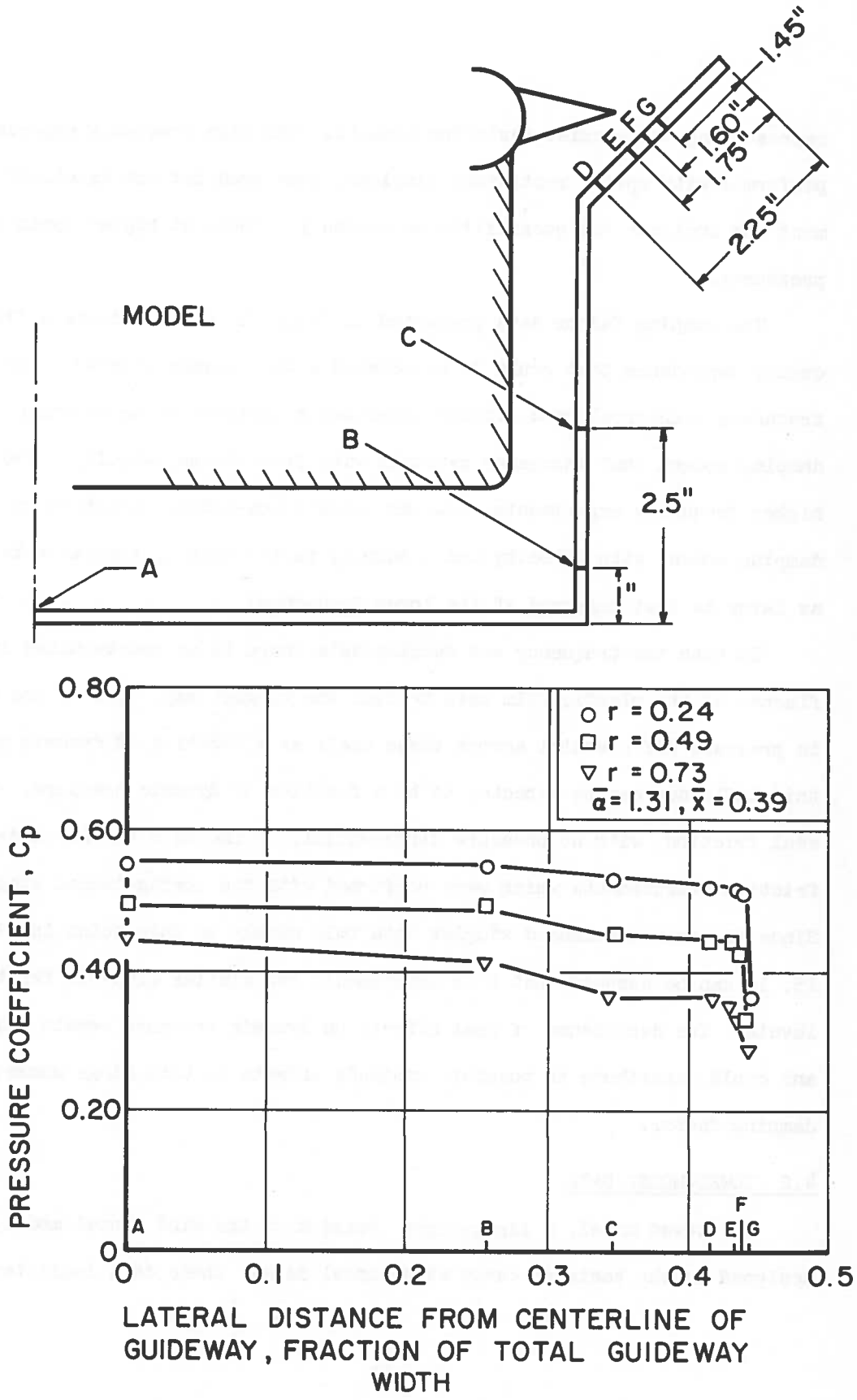

FIGURE 12b. LATERAL PRESSURE DISTRIBUTION, WIND TUNNEL DATA.

representing the winglet restoring moments. The high frequency experiments, performed with spring restrained winglets, show good but not excellent agreement and indicate the possibility of unsteady effects at higher dynamic pressures.

The damping factor data presented in Figure 15 also indicate a frequency dependence that could be associated with unsteady effects. The low frequency counterbalanced winglet experiments indicate an aerodynamic damping moment that increases smoothly with free-stream velocity. The higher frequency experiments, however, show a non-linear variation of damping moment with velocity and a damping factor that is typically twice as large as that measured at the lower frequency.

In both the frequency and damping data there is an undetermined influence of the plastic film used to seal the winglet gap. Due to the change in pressure differential across these seals as a function of dynamic pressure, this influence can be expected to be a function of dynamic pressure. The seal friction, with no pressure differential, is included in the wind-off friction measurements which were performed with the spring-loaded winglet. Since the counterbalanced winglet data fair nicely to this point in Figure 15, it can be assumed that both experiments had similar wind-off friction levels. The dependence of seal effects on dynamic pressure remain unknown and could contribute to possible unsteady effects in both hinge moment and damping factor.

4.2 TOWED-MODEL DATA

The towed model, a lightweight version of the wind tunnel model, was designed on the basis of early wind tunnel data. These data indicated that

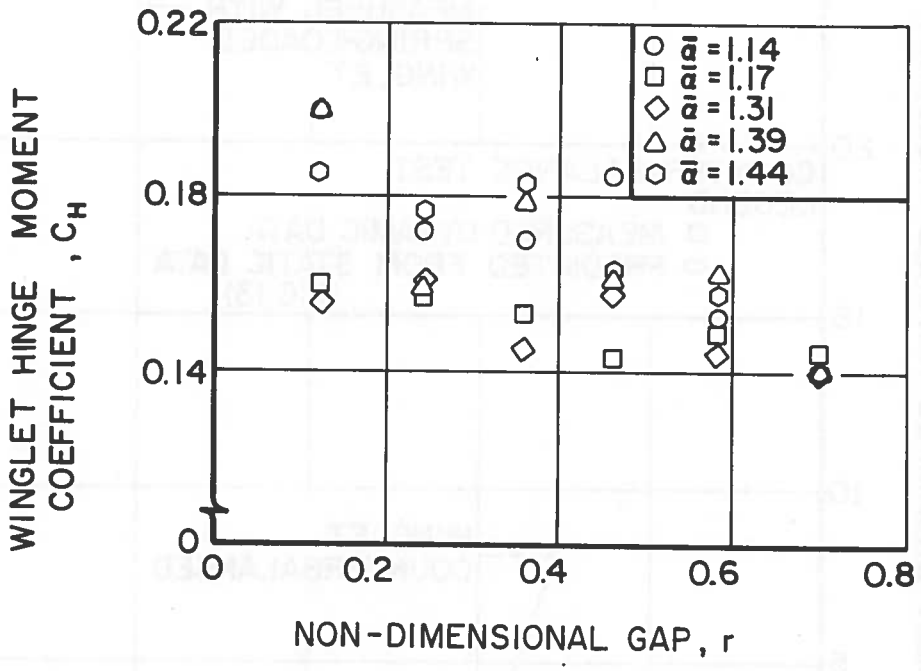

FIGURE 13. WINGLET HINGE MOMENT COEFFICIENT, WIND TUNNEL DATA.

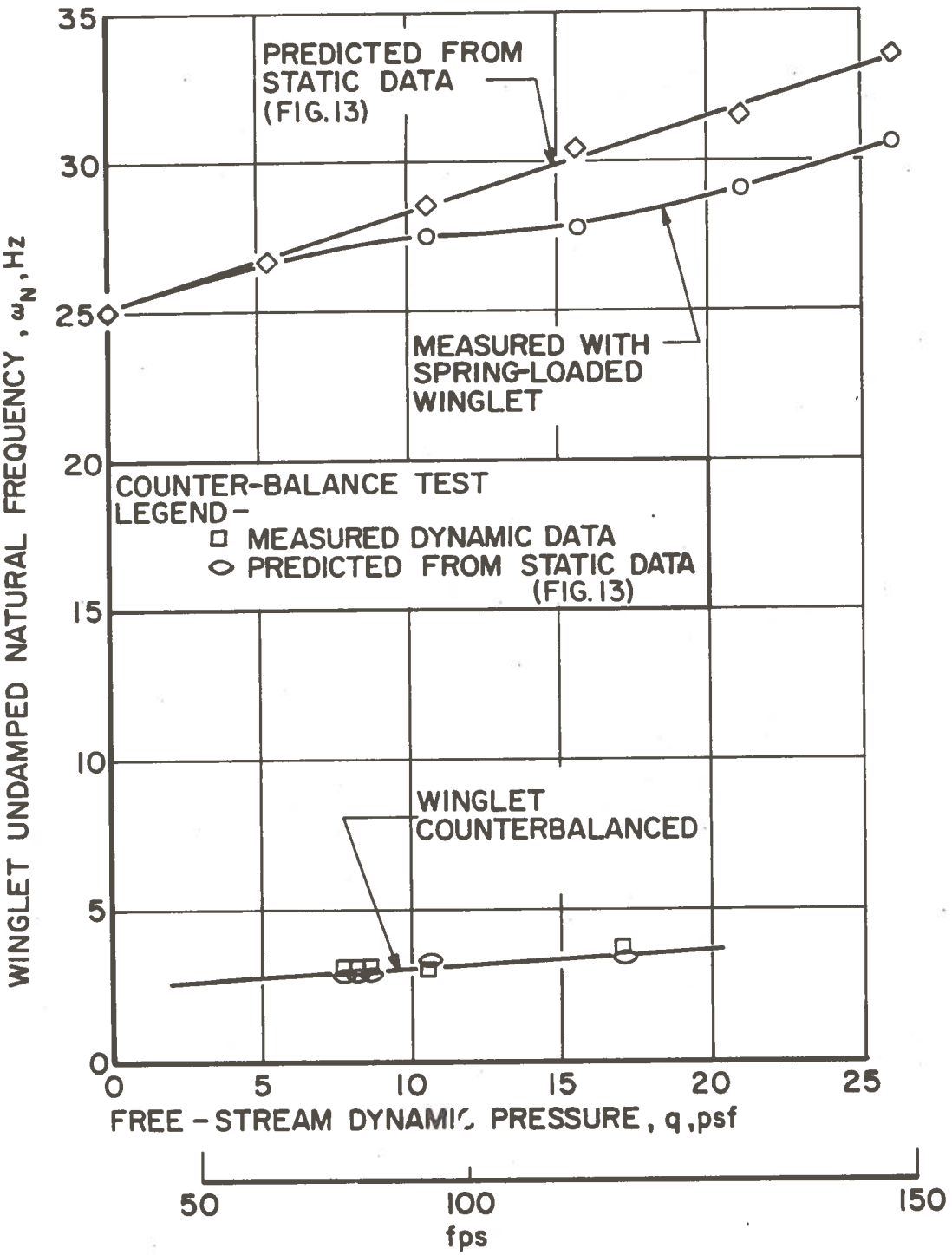

FIGURE 14. WINGLET NATURAL FREQUENCY, WIND TUNNEL DATA.

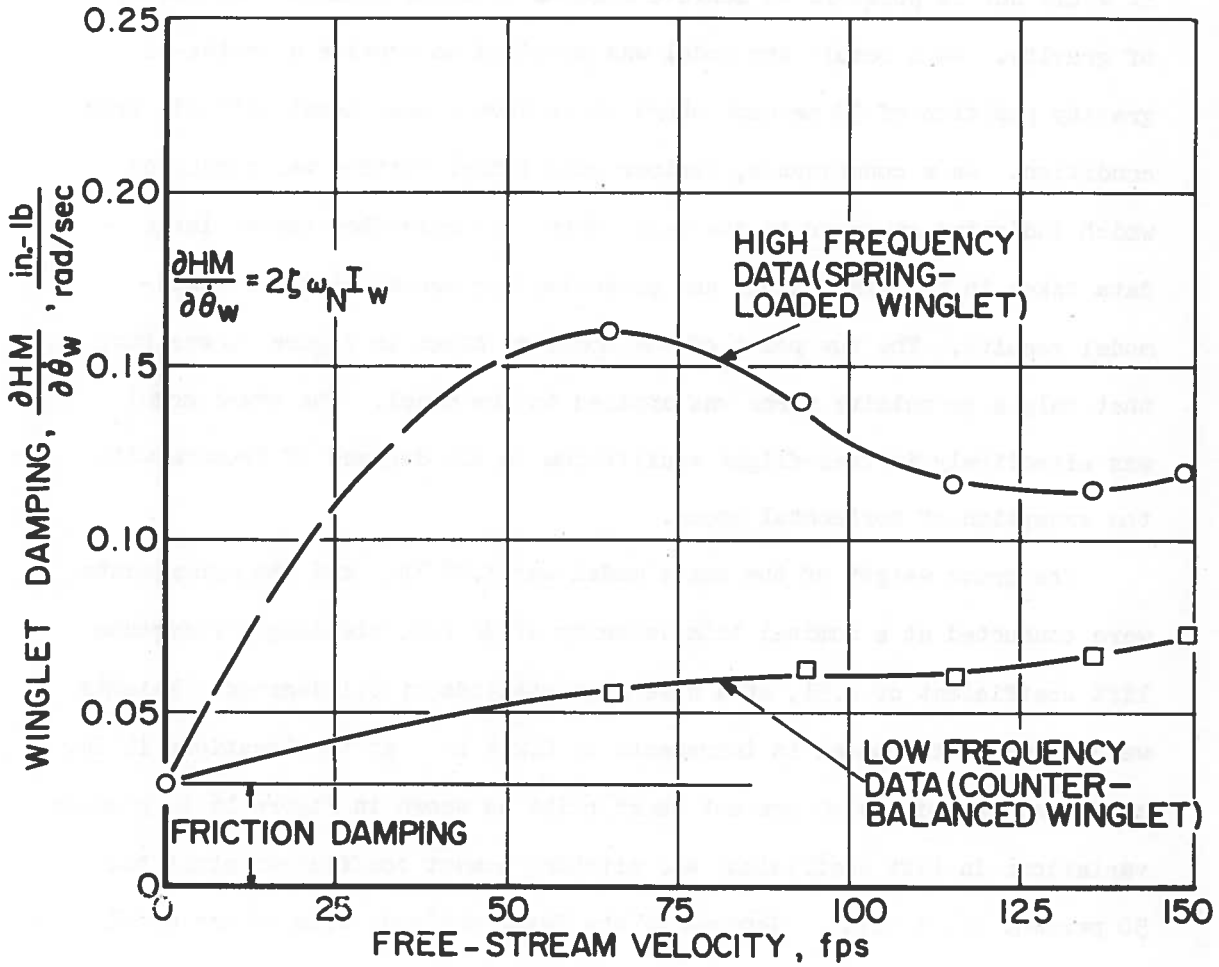

FIGURE 15. WINGLET DAMPING, WIND TUNNEL DATA.

the center of gravity of the towed model should be located at 27 percent chord. It was discovered early in the towed model experiments that this center-of-gravity position resulted in extreme model attitudes and that it would not be possible to achieve a level attitude trim at this center of gravity. As a result the model was modified to provide a center-of-gravity position of 39 percent chord which gave a near level attitude trim condition. As a consequence, further wind tunnel testing was conducted which indicated an error in the early data. As described above, later data taken in the wind tunnel and presented here agreed with the towed-model results. The tow point of the model as shown in Figure 5, was such that only a propulsive force was applied to the model. The towed model was effectively in free-flight equilibrium in all degrees of freedom with the exception of horizontal speed.

The gross weight of the basic model was 3.78 lb and the experiments were conducted at a nominal trim velocity of 32 fps, yielding a reference lift coefficient of 0.51, at a nose down attitude of 0.1 degrees. Weights were added to the model in increments of 0.214 lb at two locations 12 in. ahead and behind the 39 percent chord point as shown in Figure 16 to produce variations in lift coefficient and pitching moment coefficient about the 50 percent chord point. Generally, the level attitude trim of the model was obtained with center-of-gravity position, i.e., center-of-pressure locations, in the vicinity of 40 to 41 percent chord.

It should be noted that owing to the technique of measuring the attitude of the towed model from displacements at the leading and trailing edges, very small angular attitude variations can be measured. The full scale telemeter reading of the potentiometer/whisker system corresponded to a gap of 0.3 in. and it is estimated that this could be read within 1 percent giving measurable height variation of 0.003 in. A difference in height of 0.01 in. between the leading and trailing edges is equal to an attitude variation of 0.008 degrees. These small attitude variations can result in significant changes in the lift coefficient as shown by some recent theoretical investigations of Reference 5. Visually, of course, these small attitude variations are difficult to detect and so a considerable number of runs were necessary to obtain level attitude runs, particularly when gaining experience running the model.

Note that since the configuration of the model was fixed in the sense that the winglet deflection, with respect to the body, was constant during each series of runs, both of the dimensionless parameters, r and $\bar{\alpha}$, vary when r changes. The geometric configuration of the model is denoted by $\bar{\alpha}_N$ corresponding to a nominal value of $\bar{\alpha}$. $\bar{\alpha}_N$ is defined as the value of $\bar{\alpha}$ when the height of the winglet tip above the guideway is 0.125 in. and is uniquely determined by the winglet angle θ_w. The relationship between r and $\bar{\alpha}$ for the three values of $\bar{\alpha}_N$ examined is given in Figure 17.

As mentioned, weights were added to the model at two locations, one 12 in. forward of the 39 percent chord locations and one 12 in. aft of this point. Denoting the number of weights aft as "a" and the number of weights forward as "f", the gross weight of the model is

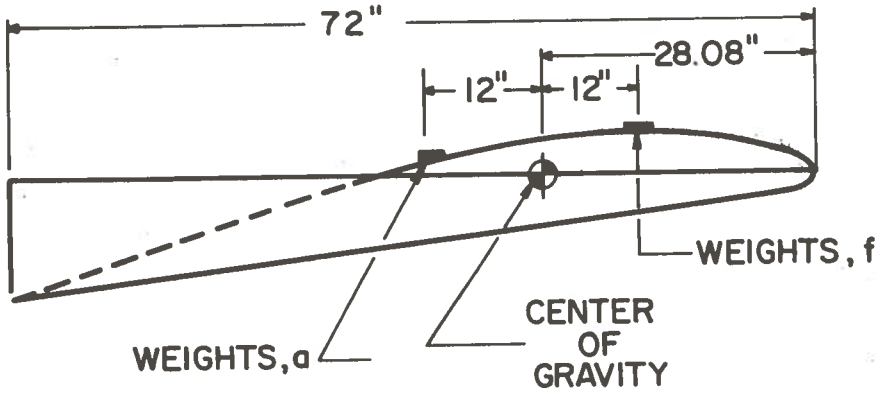

FIGURE 16. CENTER-OF-GRAVITY AND WEIGHT LOCATION, TOWED MODEL.

$$W' = W'_o + \Delta w\,(f + a)\ ,$$

and the center of gravity location measured from the leading edge of the model is given by

$$\bar{x}_{CG} = 0.39 + \frac{\Delta w\,(f - a)}{W_o' + \Delta w\,(f + a)}\ .$$

Lines on the experimental data plots in Figures 18 through 20 represent constant values of (a - f) and approximately correspond to constant center-of-gravity positions since $\Delta w \ll W'_o$. All of the data were taken at approximately constant speed.

The experimental results presented in Figure 18 through 20 show lift and pitching moment coefficients as functions of r and θ at various values of gross weight and center-of-gravity position. Lines of constant (a - f) are shown on these figures which correspond to constant center-of-pressure and, therefore, center-of-gravity position.

The experimental results at $\bar{\alpha}_N = 1.40$ illustrate the information contained in these data. For (a - f) = 0, corresponding to the model center-of-gravity located at 39 percent chord, the trim attitude was slightly nose down. Increasing the gap, and consequently reducing the lift coefficient causes an increase in nose down attitude. In terms of an actual vehicle in flight, increasing the trim velocity, corresponding to a reduction in lift coefficient for equilibrium, causes the vehicle to trim increasingly nose down. With the center of gravity moved aft approximately 1.5 percent chord, a nose up increment in trim resulted as well as an increase in lift coefficient at a constant value of the non-dimensional

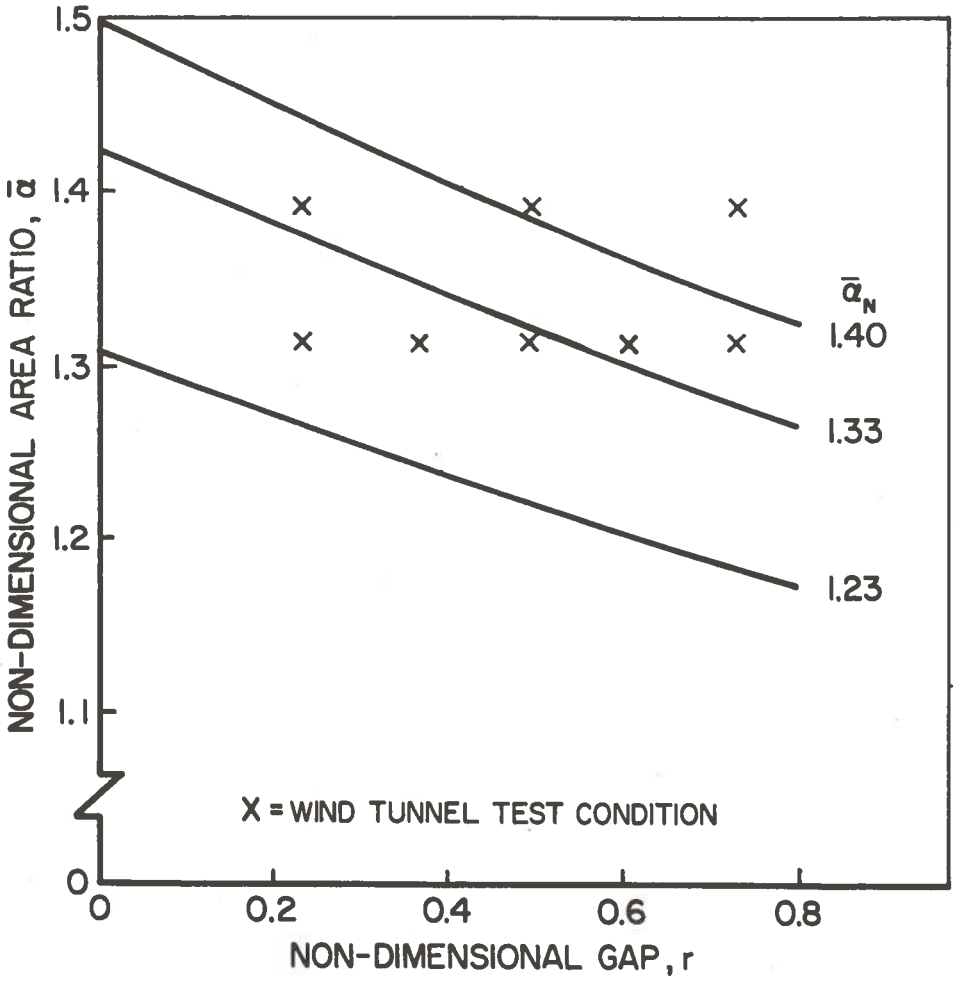

FIGURE 17. PARAMETER RELATIONSHIPS, TOWED-MODEL TESTS.

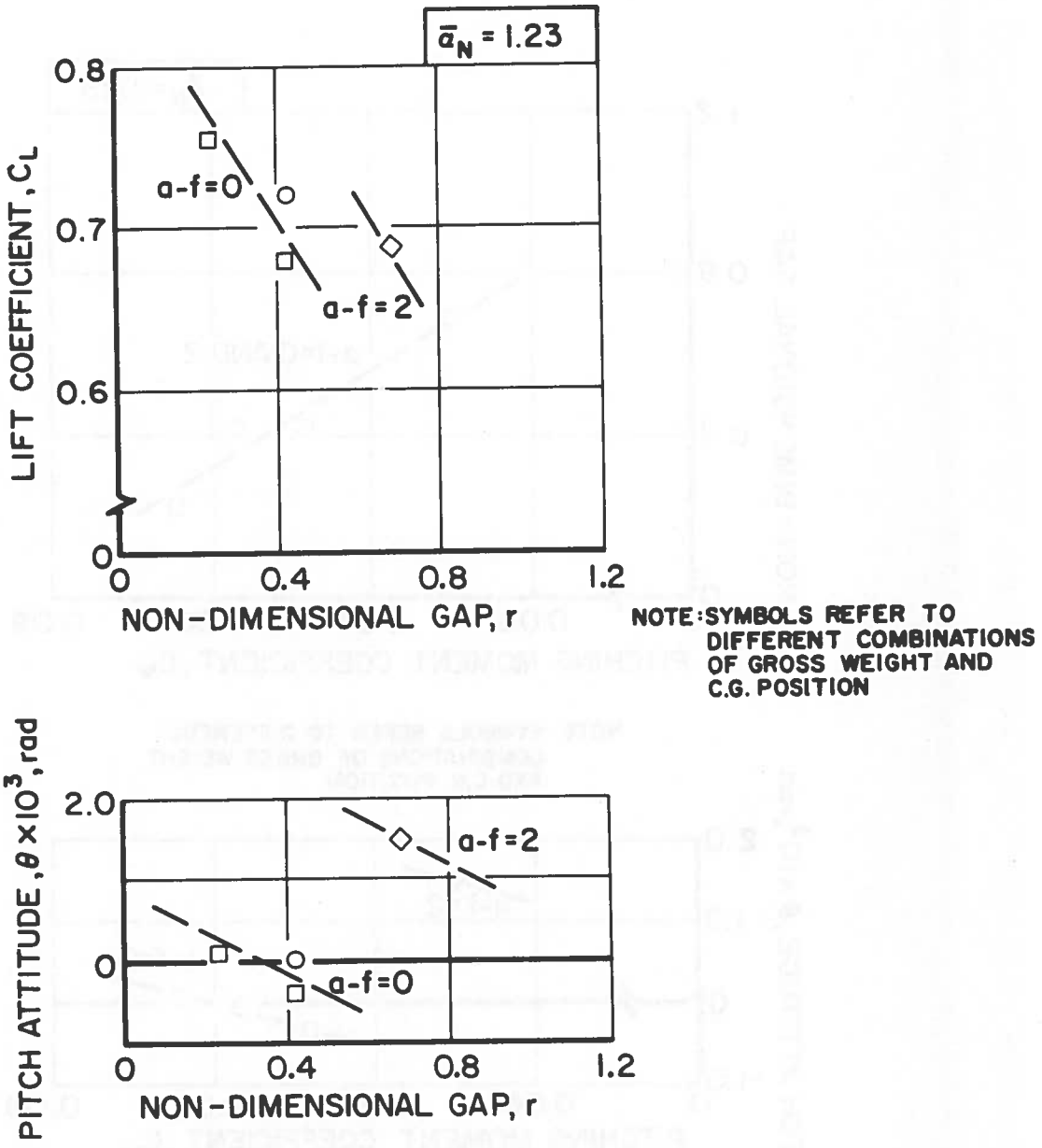

FIGURE 18. TOWED-MODEL DATA ($\bar{\alpha}_N$ = 1.23).

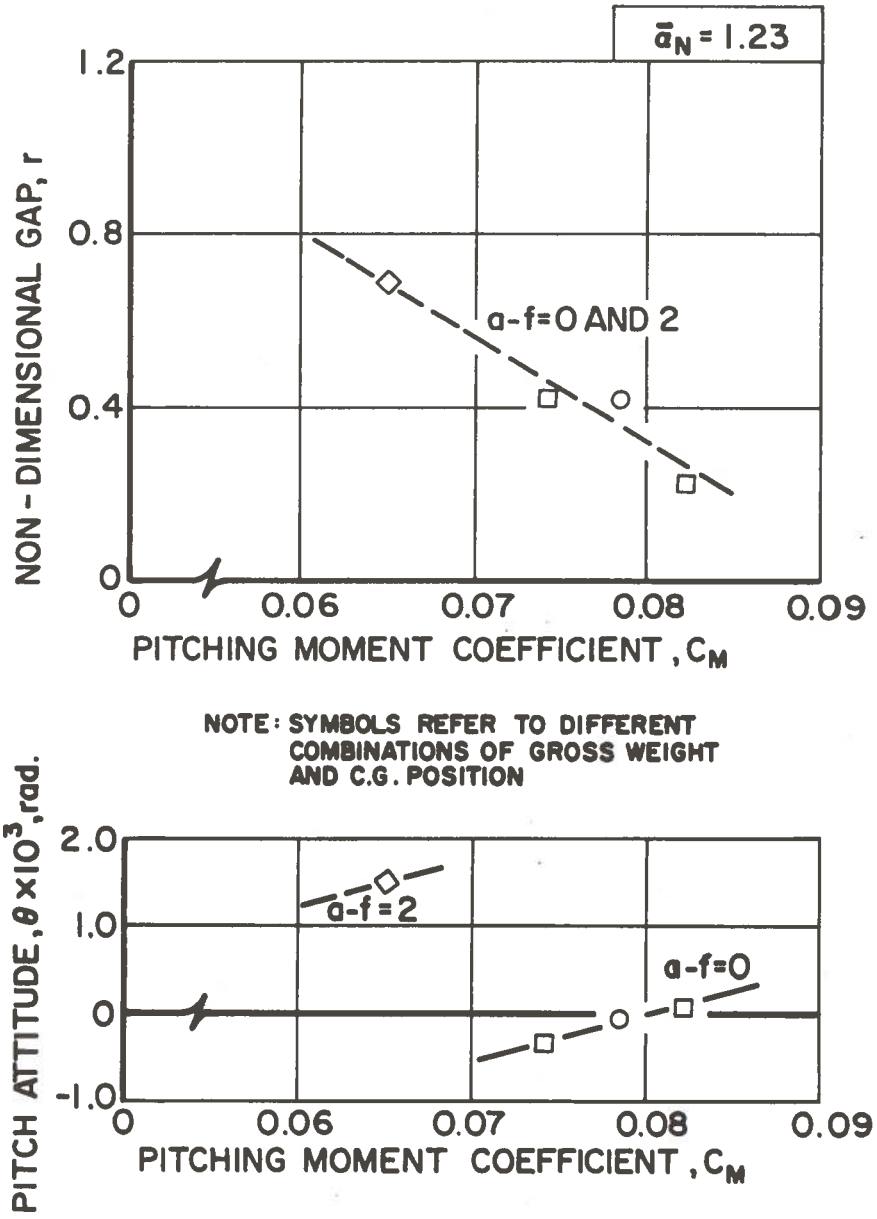

FIGURE 18. CONTINUED.

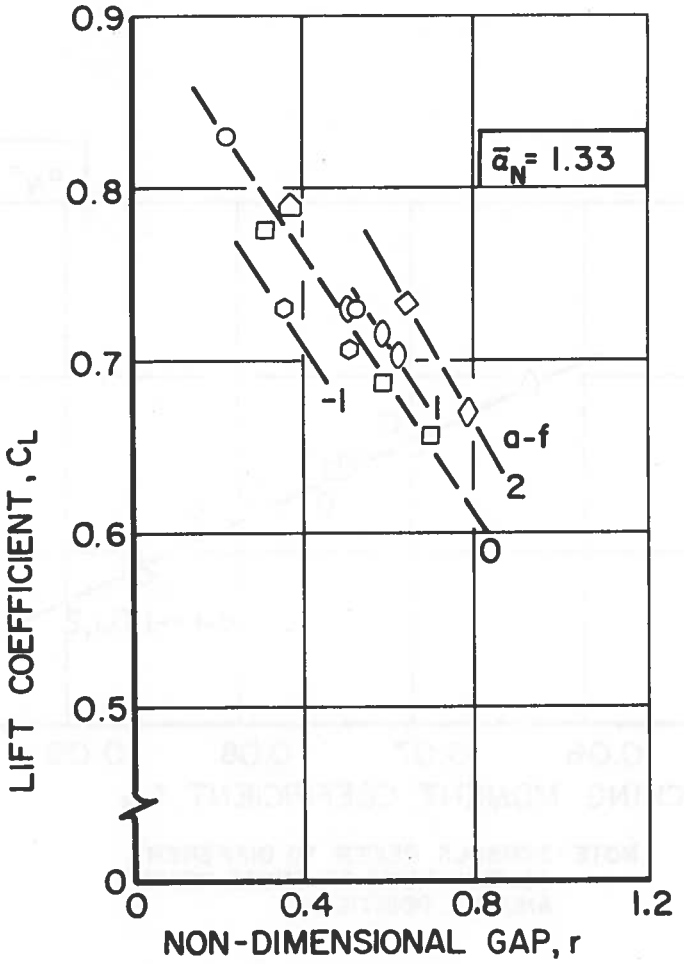

NOTE : SYMBOLS REFER TO DIFFERENT COMBINATIONS OF GROSS WEIGHT AND C.G. POSITION

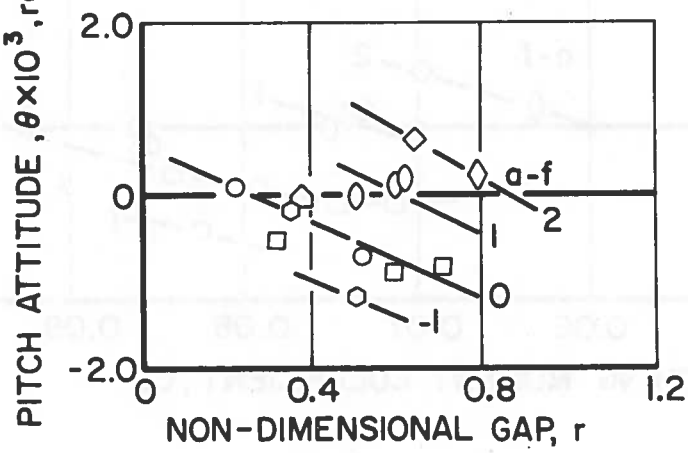

FIGURE 19. TOWED-MODEL DATA ($\bar{\alpha}_N$ = 1.33).

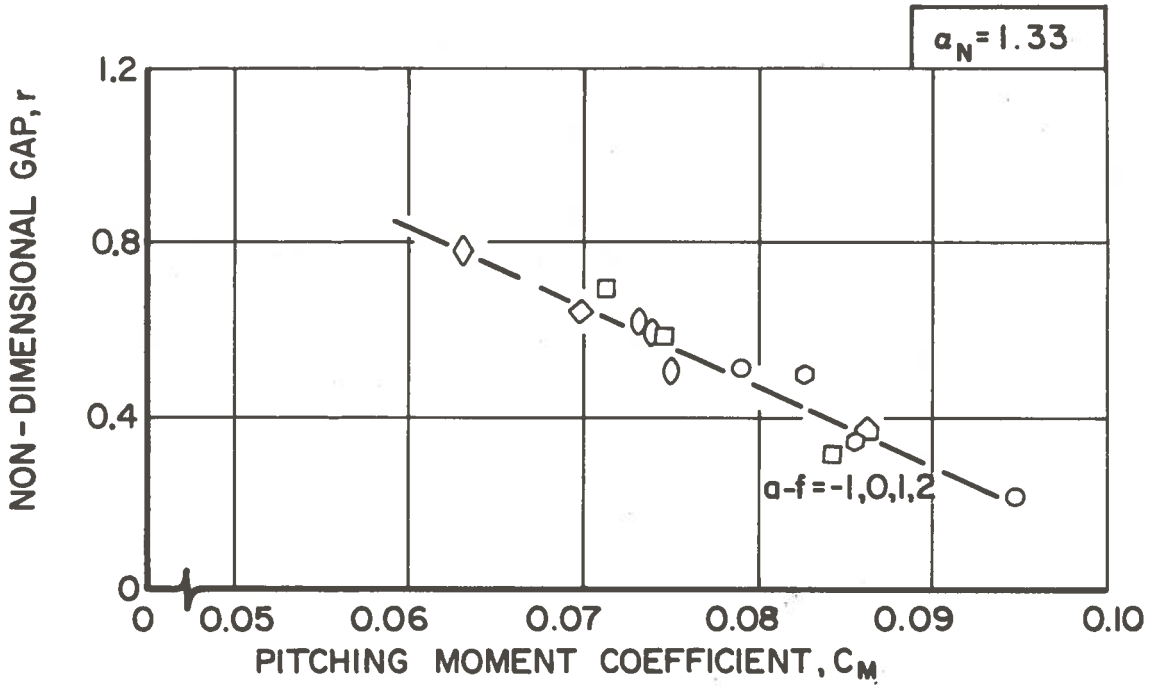

NOTE: SYMBOLS REFER TO DIFFERENT COMBINATIONS OF GROSS WEIGHT AND C.G. POSITION

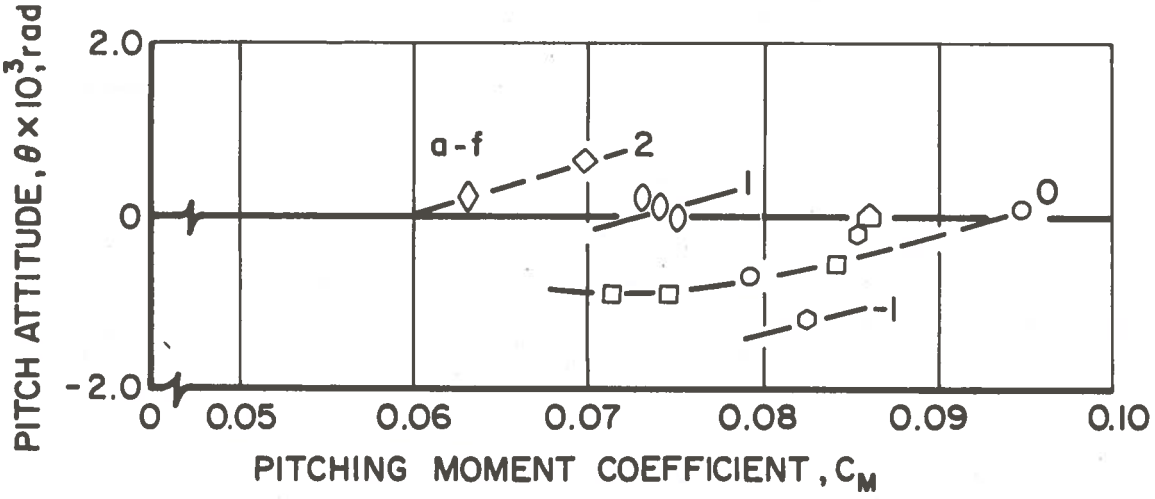

FIGURE 19. CONTINUED.

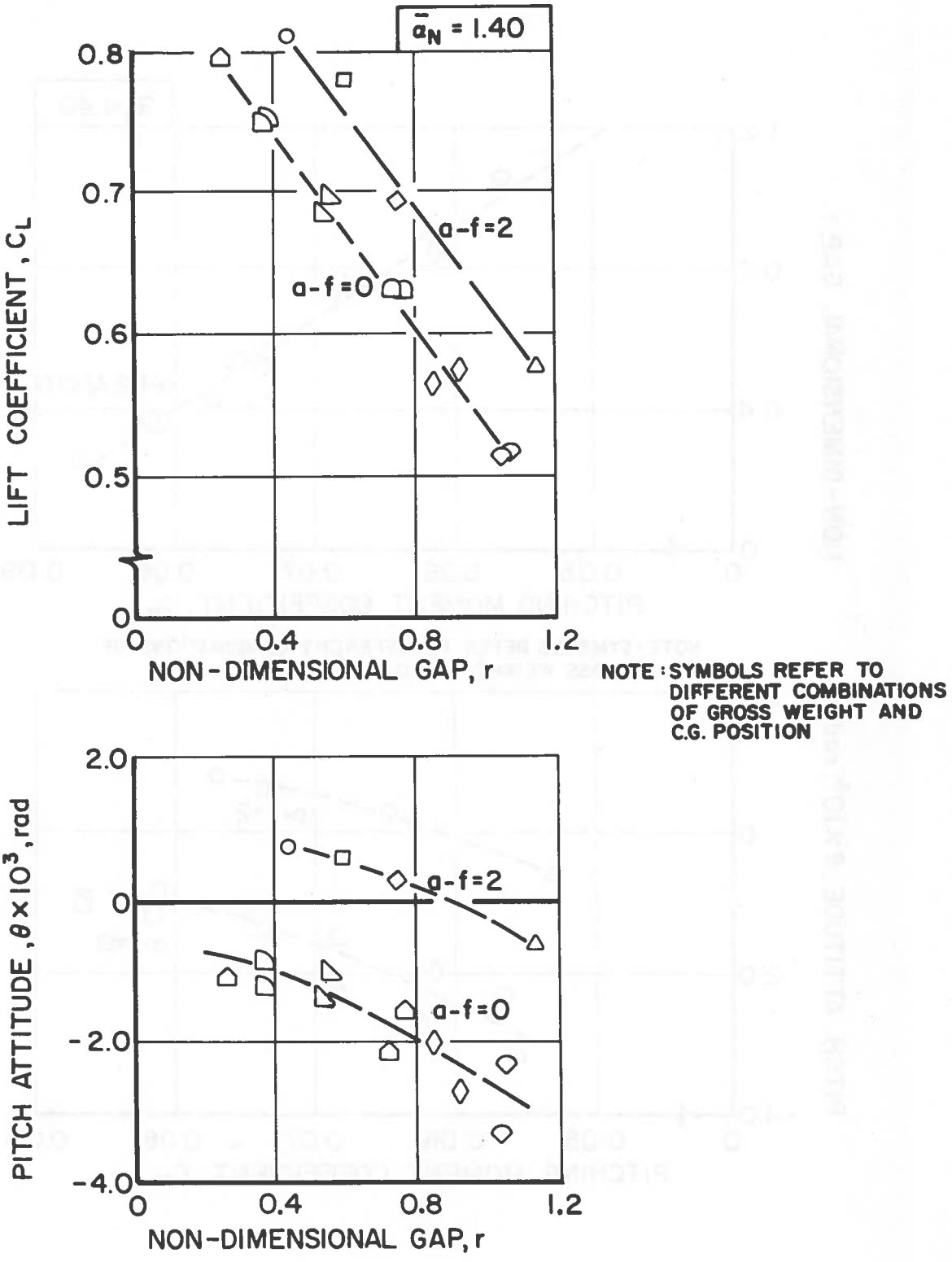

FIGURE 20. TOWED-MODEL DATA ($\bar{\alpha}_N$ = 1.40).

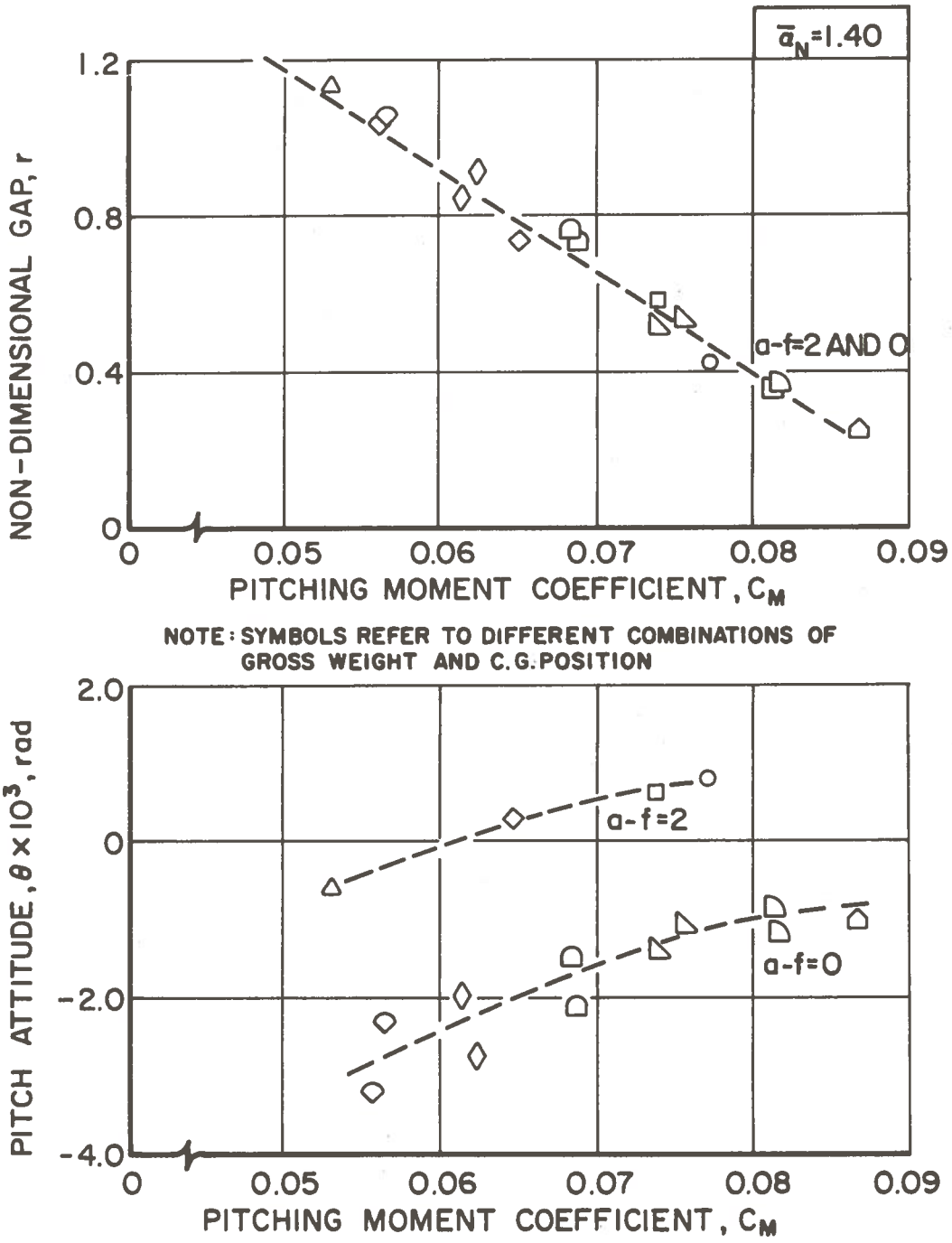

FIGURE 20. CONTINUED.

gap r. Thus, moving the center of gravity aft would result in the vehicle flying at a nose-up attitude and increased gap compared to the forward center-of-gravity location trim condition at the same speed.

At the 39 percent chord center-of-gravity location at the largest value of r, there is some scatter in the attitude-r relationship. This appeared to be a result of the model developing a lightly damped oscillation making it difficult to achieve steady-state conditions.

Since these experiments represent equilibrium flight

$$C_{\bar{M}} = 0.$$

In terms of stability derivatives, this condition may be expressed as

$$\frac{\partial C_{\bar{M}}}{\partial r} \Delta r + \frac{\partial C_{\bar{M}}}{\partial \theta} \Delta\theta = 0 \quad ,$$

or

$$\frac{\Delta\theta}{\Delta r} = - \frac{\dfrac{\partial C_{\bar{M}}}{dr}}{\dfrac{\partial C_{\bar{M}}}{\partial\theta}} \quad .$$

Thus, the slope of this equilibrium curve gives the ratio of the two pitching moment derivatives. The measured slope of the curve is negative, as shown in Figures 18 through 20, indicating that these two derivatives have the same sign. Since moving the center of gravity aft results in a nose-up attitude at a constant value of r, $C_{\bar{M}_\theta}$ evaluated with respect to the 39 percent chord point must be negative and consequently the negative slope of the equilibrium curve indicates that $C_{\bar{M}_r}$ must also be negative.

The other two $\bar{\alpha}_N$ cases examined show similar trends. Some changes in operating technique for the experiments were made during this series

of tests since the primary object was to obtain data for correlation with the wind tunnel tests.

The interpretation of these curves, to determine the stability derivatives of the vehicle, is discussed in some detail in Appendix B and the results are compared with wind tunnel test results and with theory in the following section.

5. COMPARISON OF EXPERIMENT AND THEORY

This section examines the comparison of the various experimental data obtained from the wind tunnel and towed-model tests with theory.

The theory which is presented in Appendix A is a one-dimensional theory for predicting the pressure distribution along the longitudinal axis of the model on the lower surface of the model.

A contribution from the upper surface is also included based on the assumption that the upper surface acts independently from the lower surface. It was therefore assumed that the upper surface pressure distribution on this "half" airfoil could be calculated from potential flow theory using the local velocity distribution for an NACA 0021 airfoil as given in Reference 6. The calculation of this contribution is explained in detail in Reference 5. The assumption that the upper surface acts independently of the lower surface implies that the upper surface contributions are independent of the parameters r and $\bar{\alpha}$, and are constant values given by

$$\Delta C_{L_{us}} = 0.315 \quad ,$$

$$\Delta C_{M_{us}} = 0.053 \quad .$$

The total lift and pitching moment coefficients are found by adding these values to the lower surface contribution determined from the theory of Appendix A.

5.1 PRESSURE DISTRIBUTION

Figure 21 shows a comparison of the pressure distribution along the longitudinal axis of the model determined in the wind tunnel tests with

theory. This comparison is typical of all the cases examined. The theory predicts the pressure coefficient quite well over the forward 40 percent of the lower surface and indicates a somewhat higher pressure over the aft end of the surface as compared to the experimental results. All of the experimental results indicated a small suction at the trailing edge. The theory assumes that the pressure at the trailing edge is free-stream. This difference between the measured and predicted pressure distribution is of course reflected in the lift and pitching moment prediction discussed below.

5.2 LIFT COEFFICIENT

Figure 22a presents the results of the towed-model experiments for lift coefficient. Interpolations of these data as indicated by the dashed lines were made to provide data at values of $\bar{\alpha}$ corresponding to the wind tunnel experiments. In Figure 22b these interpolated results are compared with the theory of Appendix A and the wind tunnel results presented in Figure 10. The towed-model tests show excellent agreement with theory. The lift coefficients measured in the wind tunnel are slightly larger than those obtained from the towed-model experiments and the theory, but the C_{L_r} derivative agreement is quite good. Figure 22c shows a breakdown of the estimates of the upper and lower surface contributions obtained from the theory along with the lower surface contribution obtained from integration of the pressure distributions given in Figure 12. The theory predicts a larger contribution from the lower surface as would be expected

from the pressure comparison shown in Figure 21. These results indicate that the upper surface lift is somewhat underestimated and compensates for the difference in lower surface theory and experiment giving good overall agreement. It is interesting to note that the theory and experiment are in excellent agreement with respect to the variation of lift coefficient with non-dimensional gap, a quantity that is of primary importance to the ride quality. The reason for the discrepancy between theory and experiment for the lower surface is not clear. It is possible that the guideway boundary layer contributes to this difference between theory and experiment. It is also possible that there is a difference between the pressures on the model and on the guideway. Recall that the pressures are actually measured on the guideway.

Generally speaking, all of the experimental data for lift coefficient show excellent agreement with theory for the C_{L_r} derivative. Experimental values of $C_{L_{\dot{\alpha}}}$ from both the wind tunnel and the towed model tests are about 0.26, while the theoretical prediction is approximately one-half of this value. As indicated elsewhere, this discrepancy is of less concern with regard to prediction of ride quality owing to the small influence of this derivative on the overall heave characteristics.

5.3 PITCHING MOMENT COEFFICIENT

The comparison of wind tunnel experiment, towed-model experiment and theoretical prediction of pitching moment coefficient shown in Figure 23a indicates reasonable agreement from the three sources. The wind tunnel data show a slightly more positive (nose-up) pitching moment than do the towed-model data, and the theory predicts a larger positive pitching

moment than either of the sets of data. In terms of center of pressure position, the wind tunnel data show a center of pressure at approximately 39 percent chord, (Figure 11) the towed-model data at approximately 40 percent chord and the theory predicts approximately 37 percent chord, so, in fact, the differences are rather small.

The variation of pitching moment coefficient with dimensionless gap, C_{M_r} is negative. Data from both the wind tunnel tests and towed-model tests give $C_{M_r} = 0.08$, which is quite close to the theoretical value of $C_{M_r} = 0.06$. The good agreement between theory and experiment for the variation of both the lift and pitching moment coefficients with non-dimensional gap indicates that the theoretical model which assumes that the upper surface pressure is independent of the model position in the guideway is satisfactory.

The towed model test data do not exhibit a consistent trend of C_M with $\bar{\alpha}$ and $C_{M_{\bar{\alpha}}} \cong 0$ was estimated. The wind tunnel data also indicate a very small effect. The theory predicts a value of $C_{M_{\bar{\alpha}}} \cong 0.012$.

Figure 23b shows a breakdown of the upper and lower surface contributions to the pitching moment obtained from theory of Appendix A along with the lower surface contribution obtained from the integration of the pressure distribution given in Figure 12. From this figure it can be seen that the theoretical prediction of the pitching moment contribution from the lower surface underestimates the value determined from the integration of pressures. Again, this difference would be expected from the pressure distribution comparison shown in Figure 21. The simplified theoretical model used for prediction of the upper surface pitching moment appears to overestimate the upper surface contribution.

5.4 DRAG COEFFICIENT

In Figure 24 the wind tunnel test drag coefficient data are compared with the theory of Appendix A. The theoretical curves assume a profile drag coefficient C_{D_o} Of 0.022, which is obtained by extrapolating the measured data to r = 0, corresponding to no winglet gap. The predicted increase in drag with r is larger than the experimental data indicates. The theory predicts the opposite trend with trailing edge height variation. As the trailing edge height is decreased ($\bar{\alpha}$ is increased) the theory indicates an increase in drag while the data show the opposite trend.

5.5 ATTITUDE DERIVATIVES

The pitch attitude derivatives determined from the towed model tests will be presented in a succeeding report where they will be compared with further wind tunnel results and an extended theory.

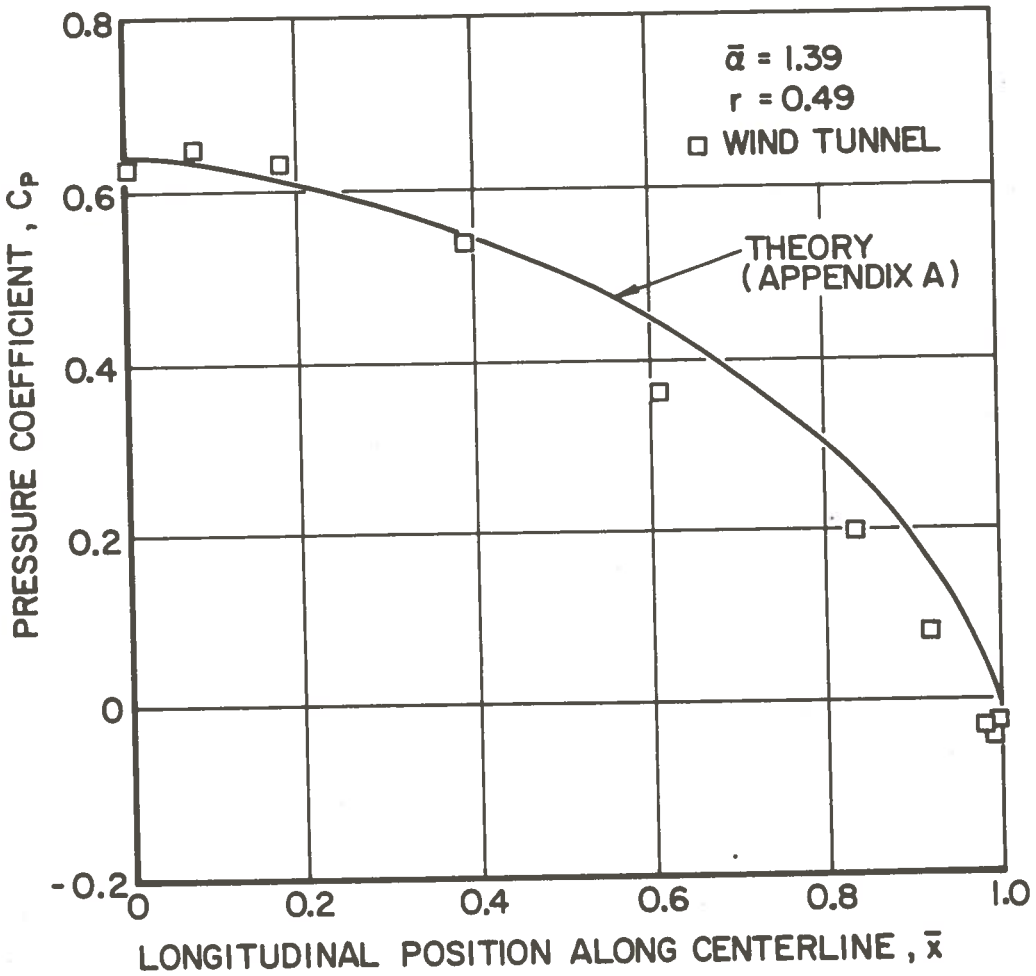

FIGURE 21. PRESSURE DISTRIBUTION, COMPARISON OF THEORY AND EXPERIMENT.

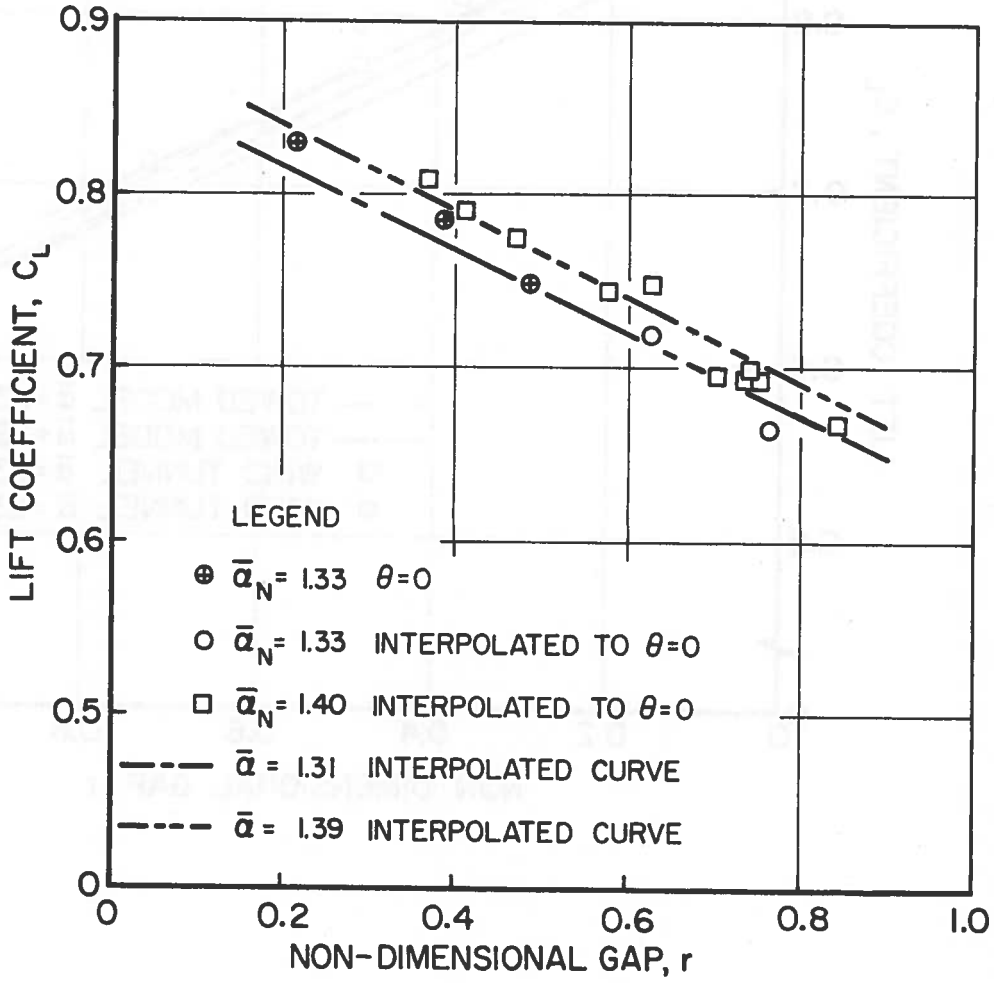

FIGURE 22a. LIFT COEFFICIENT, TOWED-MODEL DATA.

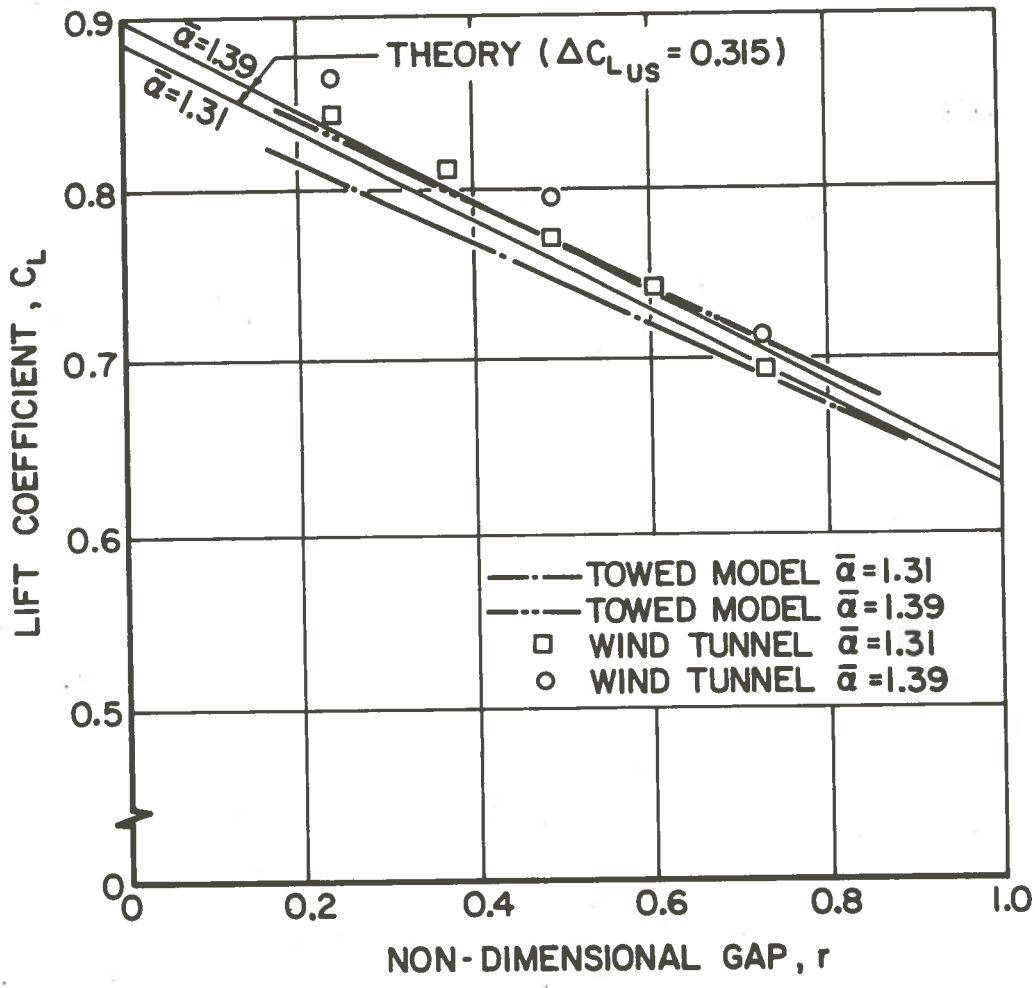

FIGURE 22b. LIFT COEFFICIENT, COMPARISON OF THEORY AND EXPERIMENT.

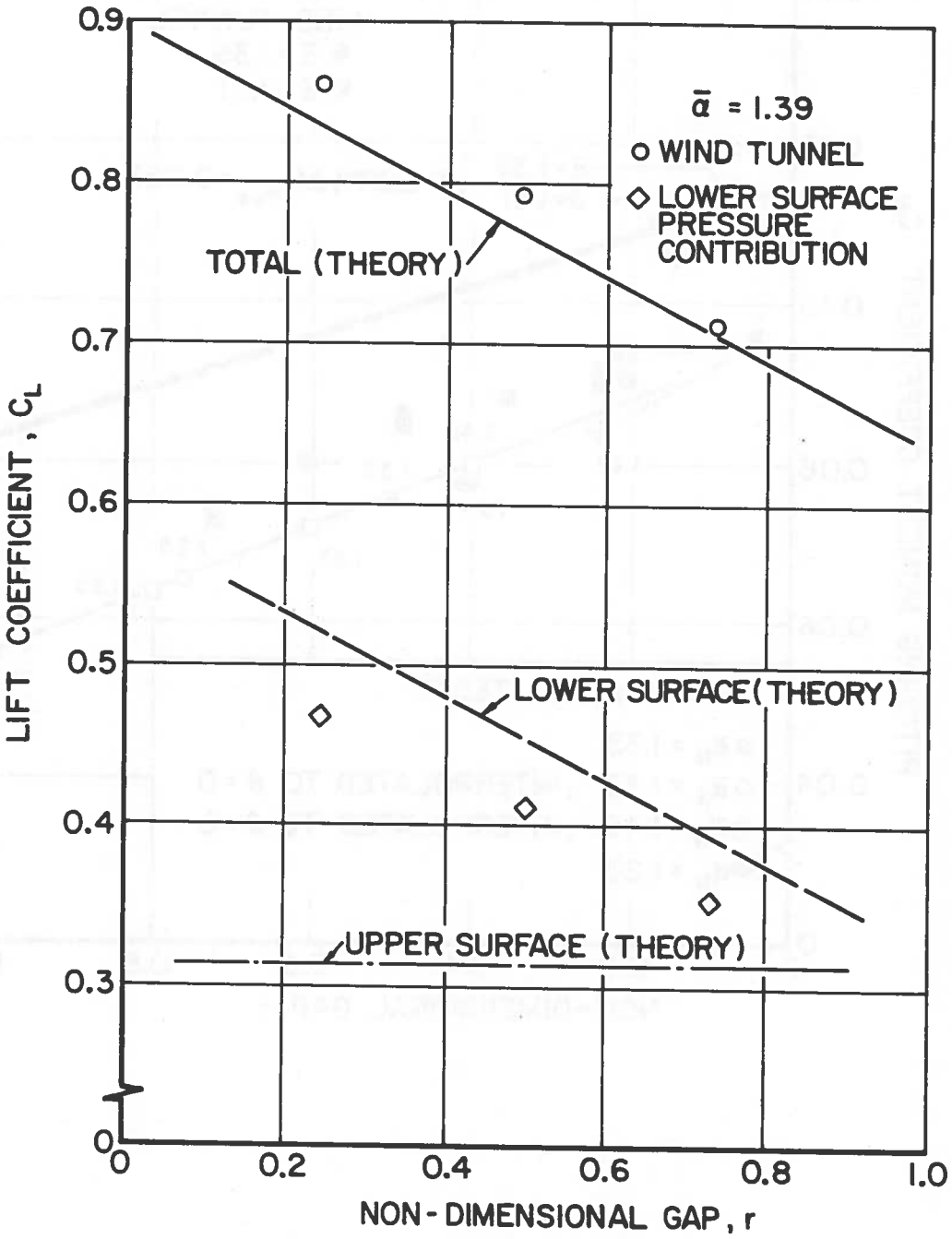

FIGURE 22c. LIFT COEFFICIENT, COMPARISON OF THEORY AND EXPERIMENT FOR UPPER AND LOWER SURFACE CONTRIBUTIONS.

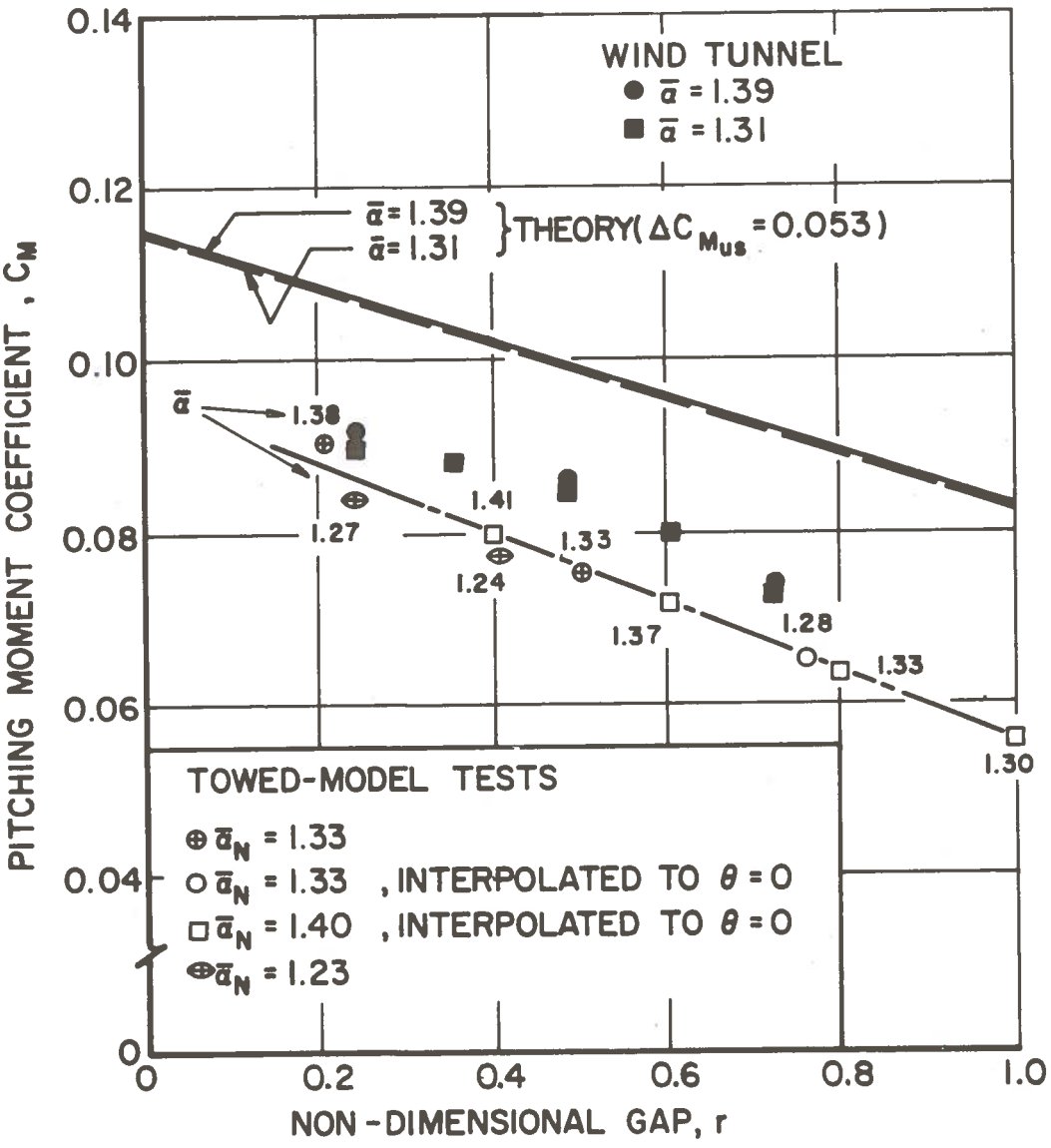

70

FIGURE 23a. PITCHING MOMENT COEFFICIENT, COMPARISON OF THEORY AND EXPERIMENT.

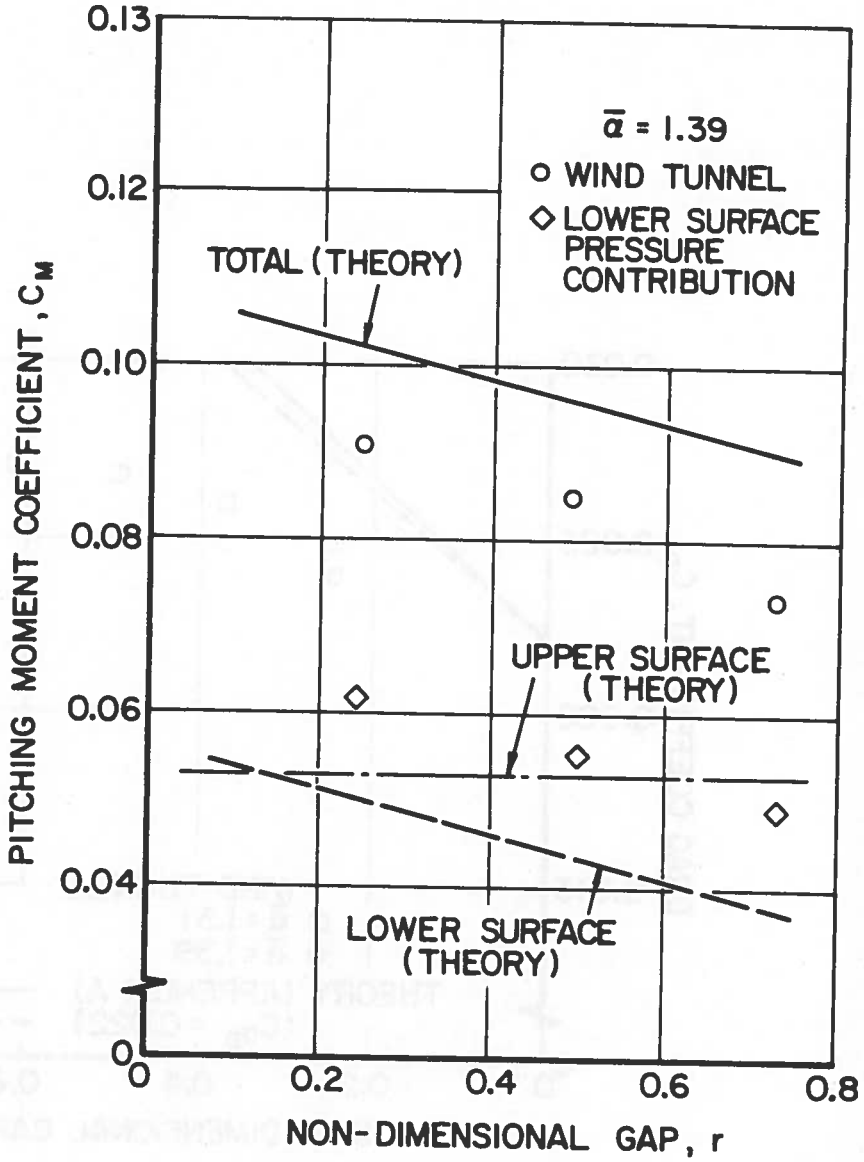

FIGURE 23b. PITCHING MOMENT COEFFICIENT, COMPARISON OF THEORY AND EXPERIMENT FOR UPPER AND LOWER SURFACE CONTRIBUTIONS.

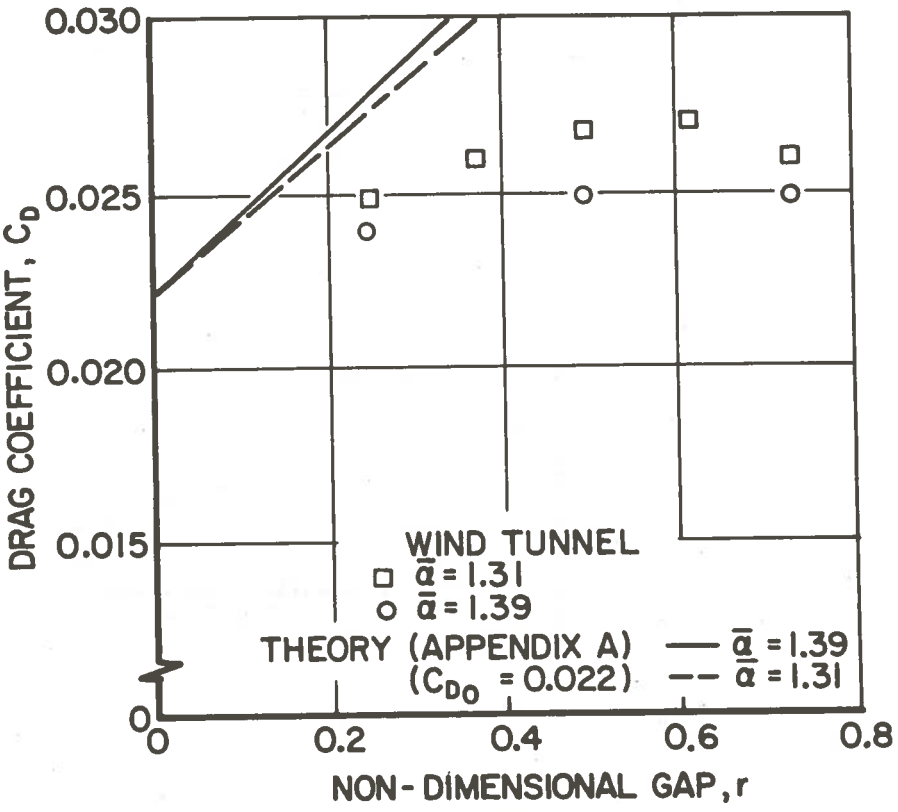

FIGURE 24. DRAG COEFFICIENT, COMPARISON OF THEORY AND EXPERIMENT.

6. CONCLUSIONS

Experiments were conducted and a theory developed to determine the longitudinal aerodynamic characteristics of a Tracked Ram Air Cushion Vehicle. Two types of experiments were conducted: one series used a model and a section of guideway in a wind tunnel; the second series employed a towed model in a 300-foot guideway.

The towed-model technique provides a better representation of the flow conditions over an actual vehicle owing to the absence of a boundary layer on the guideway, however, a higher Reynolds number can be achieved in the wind tunnel.

Wind tunnel tests are most convenient from the standpoint of data analysis and interpretation, but require considerable care in adjusting and setting the model test conditions. The towed-model experiments which were of a semi-free flight nature are relatively simple to conduct since the displacement and attitude of the model with respect to the guideway are measured as a function of model weight, center-of-gravity position and airspeed. Interpretation of the towed model data is complicated by the fact that both the attitude and height of the model change with loading. Interpretation of wind tunnel data may involve similar considerations owing to the fact that aerodynamic loading and wind tunnel balance compliance result in model deflections with respect to the guideway which can be significant as a result of the small clearances.

The experimental data taken by these two techniques agreed quite well.

Lift to drag ratios as high as 36 were measured. The towed-model experiments indicated a lift coefficient approximately 3 percent lower

than the wind tunnel results. Both sets of data indicated the same variation of lift coefficient with gap. The theory developed showed excellent agreement with the towed-model results and thus somewhat underestimated the lift coefficient measured in the wind tunnel.

The theory also gave a reasonable prediction of the pitching moment but showed poor agreement with measurements of drag coefficient in the wind tunnel, tending to overestimate the drag.

Wind tunnel testing appears to provide a satisfactory approach to the determination of the aerodynamic characteristics of Tracked Ram Air Cushion Vehicles, particularly as regards evaluation of stability derivatives.

7. RECOMMENDATIONS

Wind Tunnel Experiments on Tracked Ram Air Cushion Vehicles should include instrumentation to directly measure the relative deflection of the model/guideway system.

Additional wind tunnel data on the effect of pitch attitude on the aerodynamic characteristics is desirable.

The data presented here should be employed to conduct a study of the longitudinal dynamics and ride qualities of Tracked Ram Air Cushion Vehicles.

8. REFERENCES

1. Fraize, W. F. and Barrows, T. M.: "The Tracked Ram Air Cushion Vehicle (TRACV), A System Definition Study," The Mitre Corporation, MRT Report 6554 (PB 230 485), November 1973.

2. Barrows, T. M., Widnall, S. E. and Richardson, H. H.: "The Use of Aerodynamic Lift for Application to High Speed Ground Transportation," Report No. FRA-RT-71-56 (PB 197 242), June 1970.

3. Barrows, T. M.: "Progress on the Ram Wing Concept with Emphasis on Lateral Dynamics," Report No. DOT-TSC-FRA-71-7 (PB 210 743), June 1971.

4. Aidala, P. V.: "Lateral Stability of a Dynamic Ram Air Cushion Vehicle," Report No. FRA-ORD&D-75-6 (PB 236 516), August 1974.

5. Lee, S. D.: A Theoretical Investigation of the Aerodynamic Characteristics of a Tracked Ram Air Cushion Vehicle. Princeton University, Department of Aerospace and Mechanical Sciences, Report No. 1255-T, December 1975.

6. Abbott, I. H. and von Doenhoff, A. E.: THEORY OF WING SECTIONS, Dover Publications, New York, NY, 1959, p. 693.

7. Boccadoro, T. A.: "Towing Tank Tests on a Ram Wing in a Rectangular Guideway," Report No. FRA-RT-73-34 (PB 210 743), July 1973.

8. Barrows, T. M.: "Analytical Studies of the Lift and Roll Stability of a Ram Air Cushion Vehicle," Report No. FRA-RT-73-21 (PB 219 820), December 1972.

9. Gallington, R. W., Miller, M. K., and Smith, W. P.: "The Ram Wing Surface Effect Vehicle," Hovering Craft and Hydrofoil, Vol. 11, No. 5, 1972, p. 10-19.

NOTE: Reports with PB prefixes may be obtained from the National Technical Information Service (NTIS), Springfield, Virginia 22161.

APPENDIX A

THEORY FOR PREDICTION OF LIFT, DRAG, AND PITCHING MOMENT

In the following a simplified aerodynamic theory is developed to predict the pressure distribution on the bottom surface of a tracked ram air cushion vehicle. From the pressure distribution the contribution of the bottom surface pressure to the lift and pitching moment acting on the vehicle can be calculated. The theory is a simplified form of that developed by Boccadoro[7] and essentially involves a one-dimensional approximation to the flow field. It is particularly convenient in contrast to other results since the approximations employed lead to a closed form result for the lift coefficient. As will be indicated, over the range of parameters of interest, it agrees well with the more complex result given by Barrows[8].

The continuity equation is written for the control volume shown in Figure A-1. The upstream surface of the control volume is normal to the flow field and is located a distance x downstream from the leading edge of the vehicle and the downstream surface is located at the trailing edge of the vehicle. Mass is flowing in the upstream surface and exiting through the sides of the control volume and the downstream surface. The continuity equation for this control volume is expressed as

$$\rho A_L U = \rho A_E U_E + 2 \rho \int_x^c \delta w \, d\xi \quad . \tag{A-1}$$

It has been assumed that the velocities U and U_E are uniform across their respective areas. The velocity at the gap, w, is assumed to be only a function of distance along the body, x, and is uniform across the width of the gap. Assuming that the flow is incompressible, the density cancels out of the equation.

Differentiating this equation with respect to x yields the following differential equation which will be solved to determine the variation of gap velocity w along the vehicle

$$\frac{d(A_L U)}{dx} = - 2 \delta w \quad . \tag{A-2}$$

The boundary condition applied to this differential equation is obtained from the assumption that the pressure at the exit plane is the free-stream pressure, p_o.

Bernoulli's equation may be written as

$$p_o + \frac{1}{2} \rho V^2 = p + \frac{1}{2} \rho U^2 \quad . \tag{A-3}$$

At the exit plane $p = p_o$ and therefore

$$U(c) = V \quad . \tag{A-3a}$$

In addition, it is assumed that at the gap exit, the pressure is equal to the free-stream value. With this assumption, Bernoulli's equation may be used to relate the local velocity, U, and the gap exit velocity, w, to the free-stream velocity,

$$p_o + \frac{1}{2} \rho V^2 = p_o + \frac{1}{2} \rho (U^2 + w^2) \, . \tag{A-4}$$

Solving for the gap velocity

$$w = \sqrt{V^2 - U^2} \quad ,$$

and substituting into equation (2)

$$\frac{d(A_L U)}{dx} = - 2 \delta \sqrt{V^2 - U^2} \quad . \tag{A-5}$$

This equation is to be solved with the boundary conditon

$$U(c) = V \quad .$$

Non-dimensionalizing equation (A-5) and the boundary condition

$$\frac{dF}{d\bar{x}} = -\bar{\delta}\sqrt{1 - \bar{U}^2} \quad , \tag{A-6}$$

$$\bar{U}(1) = 1 \quad ,$$

where $F = \bar{A}\bar{U}$.

To proceed further, only the case in which the bottom surface has a uniform slope is considered so that the relationship between the dimensionless $\bar{A}$ and dimensionless distance $\bar{x}$ is

$$\bar{A} = 1 + \bar{\alpha}\,(1 - \bar{x}) \; . \tag{A-7}$$

Now the independent variable $\bar{x}$ is transformed to the variable λ, where

$$\lambda = \sqrt{\bar{A}^2 - 1} \quad ,$$

and the dependent variable is changed to

$$f = F - 1 \quad ,$$

so that equation (A-6) becomes

$$\frac{df}{d\lambda} = r\left(\frac{\lambda\sqrt{\lambda^2 - 2f - f^2}}{\lambda^2 + 1}\right) \quad , \tag{A-8}$$

with the boundary condition that

$$f(o) = 0 \quad .$$

While this differential equation can be solved exactly and the solution is given by Barrows (1972), the result is in a rather inconvenient form for obtaining a simple expression for the lift coefficient in terms of the parameters of the problem since an inverse relationship for the pressure coefficient is obtained. Therefore, an approximate solution for small r is developed. Noting that the solution of equation (A-8) for

$r = 0$ is $f = 0$, we develop an approximate solution assuming for small r that

$$f = r\, f_1 \quad ,$$

and neglecting f on the right hand side of equation (A-8)

$$\frac{df_1}{d\lambda} \cong \frac{\lambda^2}{\lambda^2 + 1} \quad . \tag{A-9}$$

Equation (A-9) can be integrated to give

$$f_1 = \lambda - \tan^{-1} \lambda \quad ,$$

and the approximate solution to equation (A-8) is therefore

$$f = r\,(\lambda - \tan^{-1} \lambda) \quad . \tag{A-10}$$

The pressure coefficient can now be determined.

From the definition of pressure coefficient,

$$C_p = 1 - \bar{U}^2 \, .$$

Expressed in terms of the above notation, where f^2 has been neglected, the pressure coefficient is,

$$C_p = \frac{\lambda^2 - 2f}{\lambda^2 + 1} \quad . \tag{A-11}$$

Substituting the value of f given in equation (A-10)

$$C_p = \frac{\lambda^2}{\lambda^2 + 1} - \frac{2\, r\,(\lambda - \tan^{-1} \lambda)}{\lambda^2 + 1} \quad . \tag{A-12}$$

Figures A-2 compares the result given in equation (A-12) with the exact solution of equation (A-8) presented in Figures 2 to 6 of Barrows (1972). It can be seen that agreement is quite good over a reasonable range of the parameter r. The parameter $\bar{h}$ employed by Barrows is related to the

parameters used here by

$$\bar{h} = \sqrt{\lambda^2 + 1} \quad .$$

The contribution to the vehicle lift coefficient from the bottom surface pressure distribution is given by

$$C_L = \int_o^1 C_p \, d\bar{x} \quad ,$$

or in terms of above parameters

$$C_L = -\frac{1}{\bar{\alpha}} \int_{\{(1+\bar{\alpha})^2 - 1\}^{\frac{1}{2}}}^{o} C_p \left(\frac{\lambda d\lambda}{\sqrt{\lambda^2 + 1}} \right) \quad . \qquad \text{(A-13)}$$

Substituting for C_p from equation (A-12)

$$C_L = \frac{\bar{\alpha}}{1 + \bar{\alpha}} - \frac{2r}{\bar{\alpha}} \int_o^{\{(1+\bar{\alpha})^2 - 1\}^{\frac{1}{2}}} \frac{(\lambda - \tan^{-1}\lambda)\,\lambda d\lambda}{(\lambda^2 + 1)^{3/2}} \quad . \qquad \text{(A-14)}$$

While the second integration can be directly performed as shown by Barrows in a private communication, it is convenient for our purposes to denote it as I and display its value graphically in Figure A-3, where

$$I(\bar{\alpha}) \equiv 2 \int_o^{\{(1+\bar{\alpha})^2 - 1\}^{\frac{1}{2}}} \frac{(\lambda - \tan^{-1}\lambda)\,\lambda d\lambda}{(\lambda^2 + 1)^{3/2}} \quad , \qquad \text{(A-15)}$$

so that the expression for the lift coefficient is

$$C_L = \frac{\bar{\alpha}}{1 + \bar{\alpha}} - \frac{r}{\bar{\alpha}} \, I(\bar{\alpha}) \quad . \qquad \text{(A-16)}$$

Figure A-4 shows graphically the dependence of the lift coefficient on the

two parameters $\bar{\alpha}$ and r determined from equation (A-16).

The contribution of the bottom surface pressure to the pitching moment coefficient may also be readily calculated. Defining a positive pitching moment as a nose up moment, the pitching moment about the leading edge is

$$C_{M_o} = -\int_o^1 C_p \bar{x} d\bar{x} \quad . \tag{A-17}$$

The pressure coefficient is given by equation (A-12). Again it is convenient to convert the variable $\bar{x}$ to λ so that this expression becomes

$$C_{M_o} = \int_{[(1+\bar{\alpha})^2 - 1]^{\frac{1}{2}}}^{o} C_p \left(\frac{\bar{\alpha} + 1}{\bar{\alpha}} - \frac{\sqrt{\lambda^2 + 1}}{\bar{\alpha}} \right) \frac{\lambda d\lambda}{\bar{\alpha} \sqrt{\lambda^2 + 1}} \quad . \tag{A-18}$$

The first term in this expression is directly related to the lift coefficient and so this expression can be written as

$$C_{M_o} = -\left(\frac{\bar{\alpha} + 1}{\bar{\alpha}} \right) C_L + \frac{1}{\bar{\alpha}^2} \int_o^{[(1+\bar{\alpha})^2 - 1]^{\frac{1}{2}}} C_p \lambda d\lambda \quad . \tag{A-19}$$

Substituting from equation (A-12) for C_p and integrating, and inserting limits, the expression for the pitching moment coefficient is

$$C_{M_o} = -\left(\frac{\bar{\alpha} + 1}{\bar{\alpha}} \right) C_L + \frac{2 + \bar{\alpha}}{2\bar{\alpha}} - \frac{1}{\bar{\alpha}^2} \ln (1 + \bar{\alpha}) - \frac{2r}{\bar{\alpha}^2} \int_o^{[(1+\bar{\alpha})^2 - 1]^{\frac{1}{2}}} \frac{\lambda (\lambda - \tan^{-1} \lambda) d\lambda}{\lambda^2 + 1} \quad . \tag{A-20}$$

Again defining the integral in the last term

$$I_M(\bar{\alpha}) \equiv 2 \int_0^{[(1+\bar{\alpha})^2 - 1]^{\frac{1}{2}}} \frac{\lambda\,(\lambda - \tan^{-1}\lambda)\,d\lambda}{\lambda^2 + 1} \quad . \qquad \text{(A-21)}$$

The dependence of this function on $\bar{\alpha}$ is shown in Figure A-5.

$$C_{M_o} = -\left(\frac{\bar{\alpha}+1}{\bar{\alpha}}\right) C_L + \frac{2+\bar{\alpha}}{2\bar{\alpha}} - \frac{1}{\bar{\alpha}^2} \ln(1+\bar{\alpha}) - \frac{r}{\bar{\alpha}^2} I_M(\bar{\alpha}). \quad \text{(A-22)}$$

This is the theoretical expression for the pitching moment coefficient about the leading edge. This can be readily transferred to the 50 percent chord point giving

$$C_M = \left(\frac{2+\bar{\alpha}}{2\bar{\alpha}}\right)(1 - C_L) - \frac{1}{\bar{\alpha}^2} \ln(1+\bar{\alpha}) - \frac{r}{\bar{\alpha}^2} I_M(\bar{\alpha}) \quad . \quad \text{(A-23)}$$

The dependence of the pitching moment coefficient on the two parameters r and $\bar{\alpha}$ is shown graphically in Figure A-6.

The nature of the terms in equation (A-23) are such that care must be taken in performing numerical calculations since the result is comprised of the small differences of relatively large numbers.

These results are compared with theory in the main body of this report.

DRAG COEFFICIENT

A theory for the prediction of drag due to lift for a configuration similar to that used here has been formulated by Gallington et al[9]. Conservation of momentum is employed to compute the force necessary to produce the momentum change of the air leaking out through the gaps, which is called the momentum drag, D_m. In the present notation this becomes

$$D_m = 2\,\delta\rho c\, w\,[V - (V^2 - w^2)^{\frac{1}{2}}] \quad . \tag{A-24}$$

Gallington assumes that the pressure is constant along the chord so that it is only necessary to non-dimensionalize (A-24) to obtain the momentum drag coefficient in terms of the lower surface pressure coefficient, which is equal to C_L. When C_p varies along the chord it becomes necessary to compute the drag at each station and integrate:

$$C_{D_m} = \frac{4\delta}{W} \int_0^1 C_p^{\frac{1}{2}} [1 - (1 - C_p)^{\frac{1}{2}}]\, d\bar{x} \quad . \tag{A-25}$$

Using (A-12), a first approximation for C_p is

$$C_p = \frac{\lambda^2}{\lambda^2 + 1} \quad . \tag{A-26}$$

In terms of non-dimensional parameters we have

$$C_{D_m} = \frac{2\,\alpha\, r}{\bar{\alpha}} \int_0^{[(1+\bar{\alpha})^2 - 1]^{\frac{1}{2}}} [1 - \frac{1}{(1+\lambda^2)^{\frac{1}{2}}}] \frac{\lambda^2\, d\lambda}{1+\lambda^2} \quad , \tag{A-27}$$

which becomes

$$C_{D_m} = \frac{2\,\alpha\, r}{\bar{\alpha}} [\lambda_o - \tan^{-1}\lambda_o + \frac{\lambda_o}{(1+\bar{\alpha})} - \ln\,(1 + \bar{\alpha} + \lambda_o)], \tag{A-28}$$

where

$$\lambda_o \equiv [(1+\bar{\alpha})^2 - 1]^{\frac{1}{2}} \quad .$$

The total drag is composed of this momentum drag plus the parasite drag

$$C_D = C_{D_o} + C_{D_m} \quad . \tag{A-29}$$

In actual fact the pressures below the wing are somewhat lower than those given by (A-26). This may partially explain the fact that (A-28) tends to give a prediction for drag which is higher than the measured values. Data from the wind tunnel tests are compared with (A-28) in Figure 24.

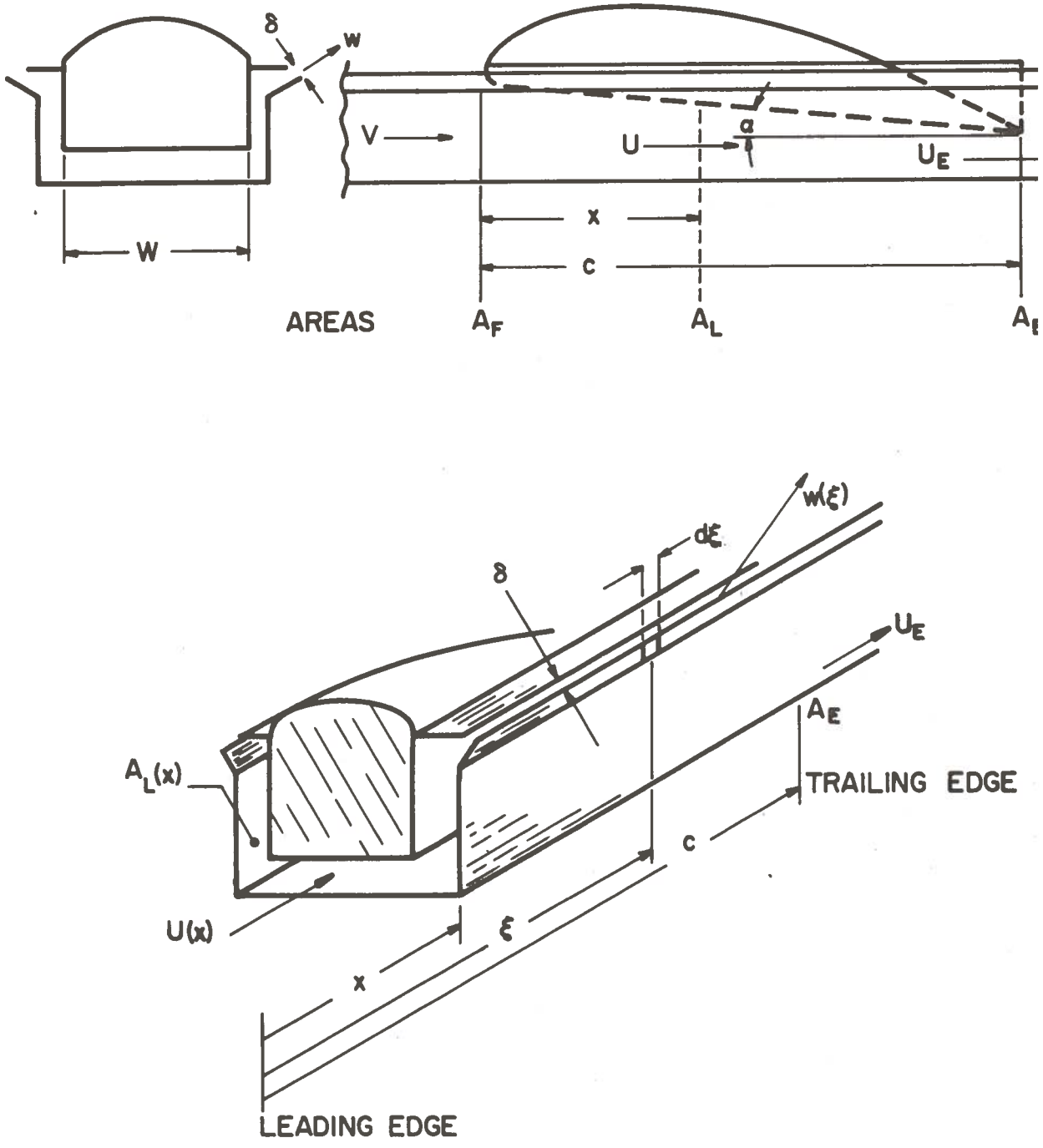

FIGURE A-1. NOMENCLATURE FOR THEORY

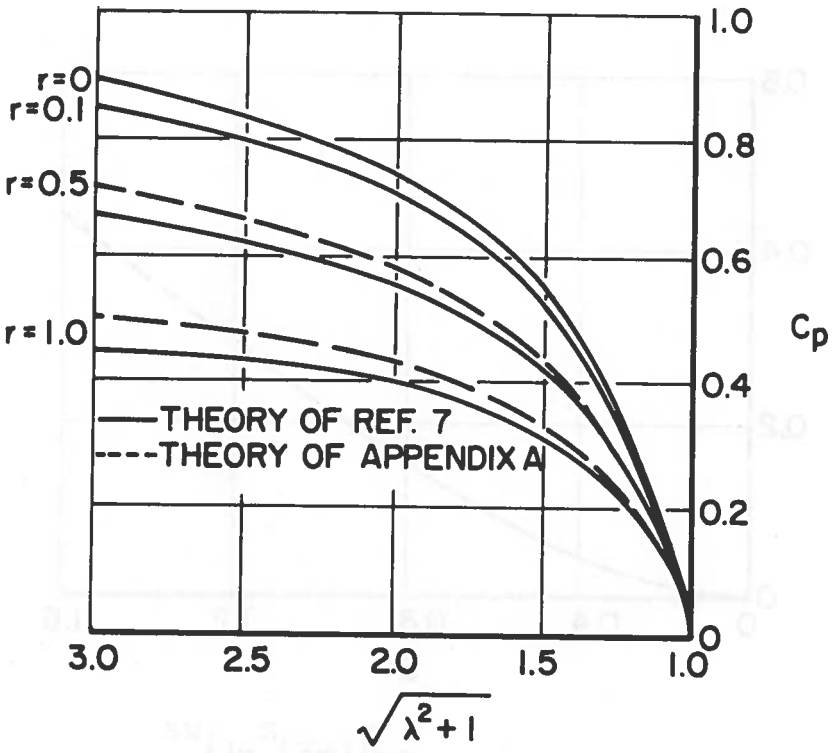

FIGURE A-2. COMPARISON OF APPROXIMATE THEORY WITH EXACT THEORY. PREDICTIONS INDISTINGUISHABLE FOR r = 0 AND 0.1.

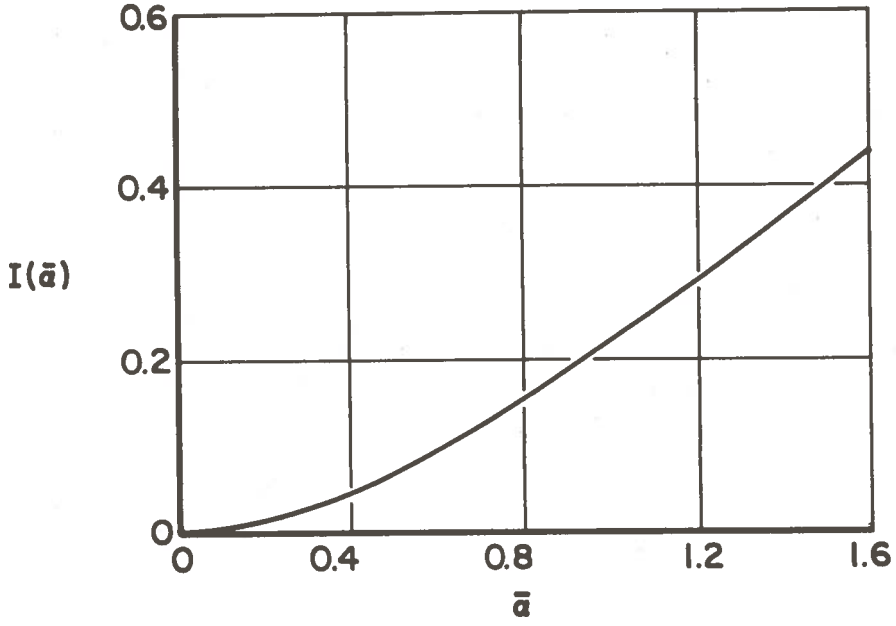

$$I(\bar{a}) = 2\int_0^{\left\{(1+\bar{a})^2-1\right\}^{1/2}} \frac{\lambda(\lambda - \mathrm{TAN}^{-1}\lambda)\,d\lambda}{(\lambda^2+1)^{3/2}}$$

FIGURE A-3. INTEGRAL FOR CALCULATION OF LIFT COEFFICIENT.

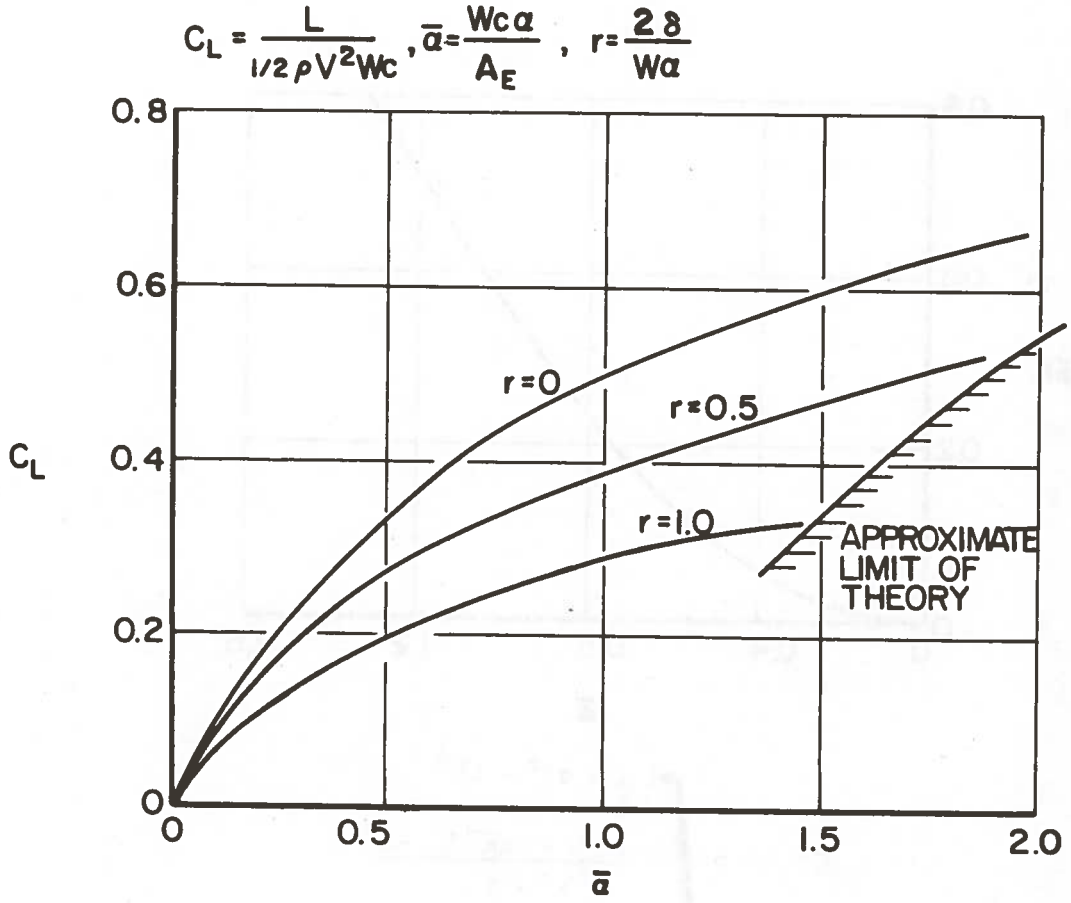

FIGURE A-4. LIFT COEFFICIENT, THEORY.

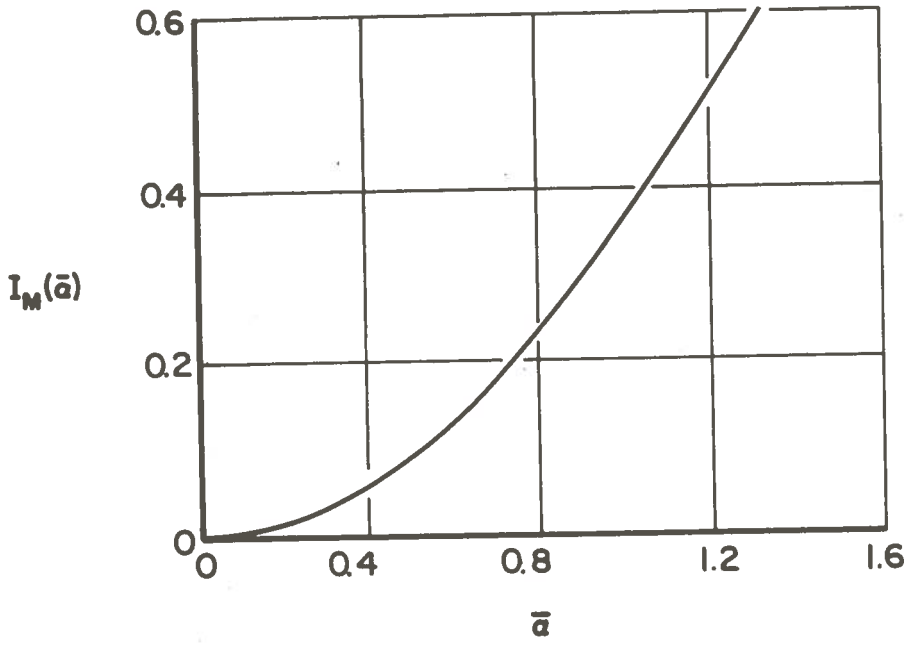

$$I_M(\bar{\alpha}) = 2 \int_0^{[(1+\bar{\alpha})^2 - 1]^{\frac{1}{2}}} \frac{\lambda \, (\lambda - \tan^{-1}\lambda) \, d\lambda}{\lambda^2 + 1}$$

FIGURE A-5. INTEGRAL FOR CALCULATION OF PITCHING MOMENT COEFFICIENT.

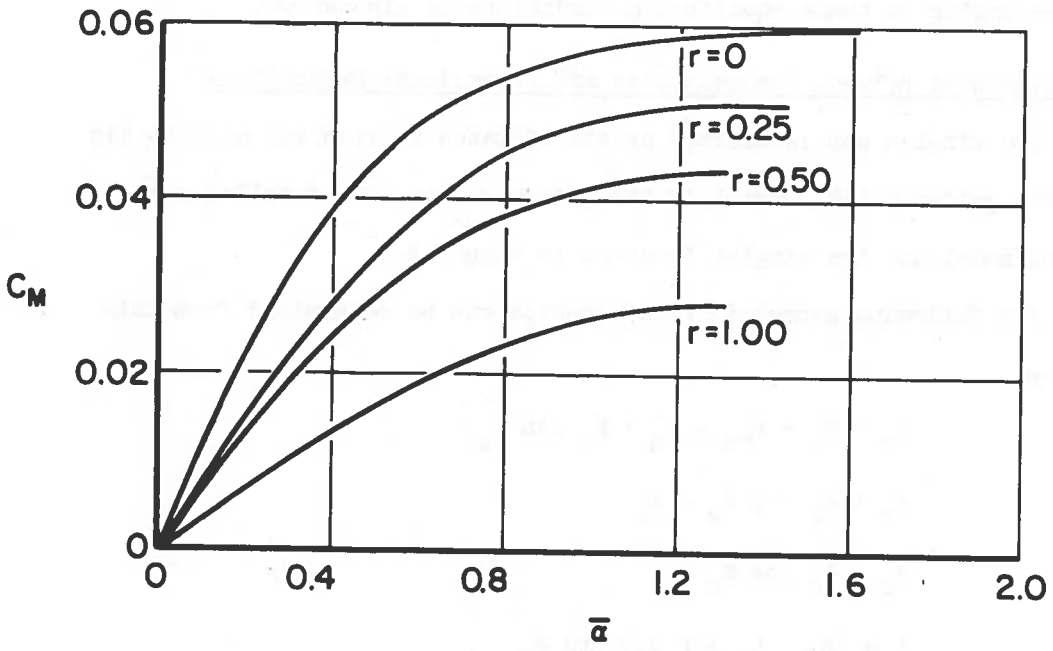

FIGURE A-6. PITCHING MOMENT COEFFICIENT, THEORY.

APPENDIX B

DETERMINATION OF LIFT AND PITCHING MOMENT DERIVATIVES FROM TOWED-MODEL EXPERIMENTS

The towed-model tests involve the measurement of the equilibrium position of the model with respect to the guideway, as a function of model weight and center-of-gravity position. This equilibrium condition expressed in terms of the non-dimensional gap, r, and the attitude of the model, θ, has been shown in Figures 18 through 20. The loading condition, expressed in terms of lift coefficient and pitching moment coefficient, corresponding to these equilibrium conditions is also shown.

Relationships Between Dimensionless and Dimensional Derivatives

The winglet gap is defined as the distance between the winglet tip and the guideway lip, normal to the guideway lip. The detailed geometry of the model and the winglet is shown in Figure B-1.

The following geometric relationships can be determined from this figure

$$Z_T = Z_w + h_{TE} - h_G + \ell_w \sin \theta_w$$

$$s_T = \ell_w \cos \theta_w - s_w$$

$$s_T = \ell_G \cos \phi_G$$

$$\delta = (Z_T - \ell_G \sin \phi_G) \cos \phi_G \quad .$$

With some algebra, the winglet gap can be related to the winglet deflection angle with respect to the vehicle and the trailing edge height as

$$\delta = \{Z_w + s_w \tan \phi_G - h_G + h_{TE} + \ell_w (\sin \theta_w - \tan \phi_G \cos \theta_w)\} \cos \phi_G \quad .$$

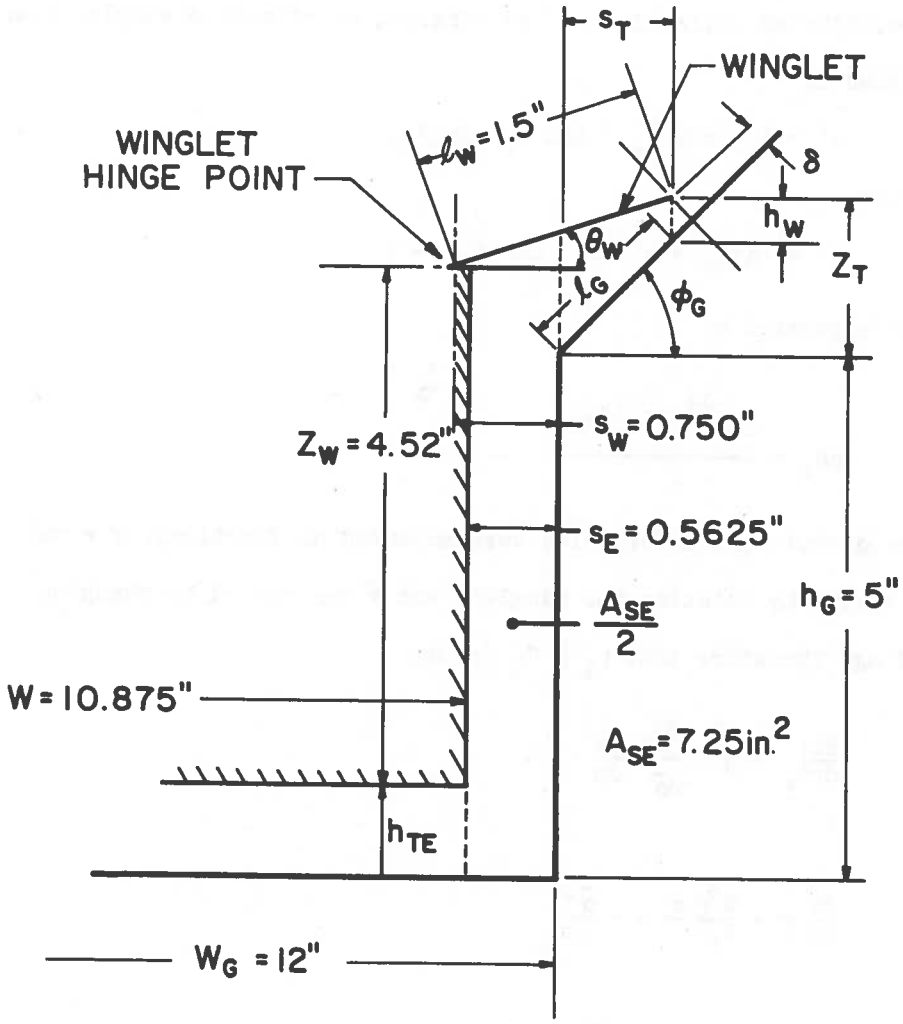

FIGURE B-1. DETAILED GEOMETRY OF WINGLET AND GUIDEWAY.

For small perturbations,

$$\Delta\delta = \Delta h_{TE} \cos \phi_G + \ell_w \cos \phi_G \, (\cos \theta_w + \tan \phi_G \sin \theta_w) \, \Delta\theta_w \, .$$

This gives the perturbation relationship between winglet gap, trailing edge height and winglet rotation when the winglet is free. Linearizing about an equilibrium deflection of the winglet, an effective winglet span may be defined as

$$e' = \ell_w \, (\cos \theta_w + \tan \phi_G \sin \theta_w) \, ,$$

and therefore

$$\Delta\delta = (\Delta h_{TE} + e' \, \Delta\theta_w) \cos \phi_G \, .$$

This may be expressed as

$$\Delta\theta_w = \frac{\frac{\Delta\delta}{\cos \phi_G} - \Delta h_{TE}}{e'} \, .$$

Now the aerodynamic characteristics were measured as functions of r and $\bar{\alpha}$. r was varied by rotating the winglet, and $\bar{\alpha}$ was varied by changing h_{TE}. Knowing, therefore that $C_L = C_L \, (r, \bar{\alpha})$

$$\left.\frac{dL}{dh}\right|_\delta = q \, S \, \frac{dC_L}{d\bar{\alpha}} \, \frac{d\bar{\alpha}}{dh} \, ,$$

and

$$\frac{d\bar{\alpha}}{dh} = - \frac{W^2 c \, \alpha}{A_E^2} = - \frac{\bar{\alpha}^2}{c \, \alpha} \, ,$$

so that

$$\left.\frac{dL}{dh}\right|_\delta = - q \, S \, \left(\frac{\bar{\alpha}^2}{c\alpha}\right) \frac{dC_L}{d\bar{\alpha}}$$

$$\left.\frac{dL}{d\delta}\right|_h = q \, S \, \frac{dC_L}{dr} \, \frac{dr}{d\delta} = q \, S \, \left(\frac{2}{W\alpha}\right) \frac{dC_L}{dr} \, .$$

The latter derivative may also be expressed in terms of winglet rotation as

$$\left.\frac{dL}{d\theta_w}\right|_h = e' \cos \phi_G \left.\frac{dL}{d\delta}\right|_h .$$

Similar relationships hold for the pitching moment derivatives.

If the winglet is held fixed with respect to the body, i.e., a rigid vehicle is considered, then

$$\Delta\theta_w = 0$$

and the winglet gap perturbation is related to a vehicle height perturbation by the relationship

$$\Delta\delta = \Delta h_{TE} \cos \phi_G ,$$

and therefore, the heave derivative for a rigid vehicle is

$$\left.\frac{dL}{dh}\right|_{\theta_w} = \left.\frac{dL}{dh}\right|_{\delta} + \left.\frac{dL}{d\delta}\right|_h \left.\frac{d\delta}{dh}\right|_{\theta_w}$$

$$= \left.\frac{dL}{dh}\right|_{\delta} + \cos \phi_G \left.\frac{dL}{d\delta}\right|_h .$$

In dimensionless form.

$$\left.\frac{dL}{dh}\right|_{\theta_w} = q\,S \left\{\frac{2}{W\alpha} \frac{dC_L}{dr} \cos \phi_G - \frac{\bar{\alpha}^2}{c\alpha} \frac{dC_L}{d\bar{\alpha}}\right\}$$

or as

$$\left.\frac{dL}{dh}\right|_{\theta_w} = \frac{qS}{W\alpha} \left\{2 \frac{dC_L}{dr} \cos \phi_G - \bar{\alpha}^2 \frac{W}{c} \frac{dC_L}{d\bar{\alpha}}\right\} .$$

This is the combination of dimensionless derivatives determined from the towed-model tests since the winglet was fixed with respect to the body in these experiments.

In the towed-model tests, the parameter $\bar{\alpha}_N$, the nominal value of $\bar{\alpha}$, is used to define the winglet angle θ_w. This gives the following relationship between $\bar{\alpha}$ and r

$$\bar{\alpha} = \frac{\bar{\alpha}_N}{1 + \frac{\bar{\alpha}_N}{\cos \phi_G} \frac{W}{c} (r - r_N)} \quad ,$$

where r_N is the value of the dimensionless parameter r corresponding to the nominal value of δ. This relationship is shown in Figure 17. The nominal value of δ corresponds to a distance between the winglet tip and the guideway measured perpendicular to the guideway lip of 0.125 in., thus $\delta_N = 0.0884$ in. and $r_N = 0.428$.

Interpretation of Towed-Model Data

The static stability derivatives of the vehicle necessary for prediction of the dynamics of the pitch/heave motion can be determined from the towed model tests in the following fashion. The lift coefficient and the pitching moment coefficient are functions of the two variables, r, and θ,

$$C_L = C_L(r,\theta)$$

$$C_M = C_M(r,\theta) \quad ,$$

and the equilibrium conditions of the model are

$$L = W'$$

$$\bar{M} = 0 \quad .$$

Expressing the pitching moment about the center of gravity, in terms of the value at a fixed reference point (0.5c)at a distance Δx, aft of the center of gravity

$$M = \bar{M} + \Delta x L \quad .$$

The lift coefficient is

$$C_L = \frac{W'}{qS} \quad .$$

and the pitching moment coefficient is

$$C_M = C_{\bar{M}} + \Delta\bar{x}\, C_L \quad .$$

The relationship between θ and r for equilibrium flight may be used to determine ratios of the static stability derivatives. A line on the graph of θ vs. r connecting points of constant lift coefficient has a slope determined from the mathematical expression that the lift coefficient is constant

$$\frac{\partial C_L}{\partial r}\Delta r + \frac{\partial C_L}{\partial \theta}\Delta\theta = 0 \quad ,$$

and therefore, a line connecting constant C_L points has the slope

$$\left.\frac{\Delta\theta}{\Delta r}\right|_{C_L} = -\frac{\frac{\partial C_L}{\partial r}}{\frac{\partial C_L}{\partial \theta}} \quad .$$

The experimental curves generally have a positive slope indicating that $\frac{\partial C_L}{\partial \theta}$ is of opposite sign to $\frac{\partial C_L}{\partial r}$.

The lift derivatives can be individually determined from the relationship between C_L and r. $\frac{\partial C_L}{\partial r}$ is given directly by considering points on the graph with the same attitude and $\frac{\partial C_L}{\partial \theta}$ may be found from points with different attitudes at the same value of r.

The slope of lines on the graph of the equilibrium relationship between θ and r at constant center-of-gravity position can be used to determine the ratio of the pitching moment derivatives in a similar fashion. In equilibrium flight

$$C_{\bar{M}} = 0 \quad .$$

Therefore, along lines of constant center-of-gravity position

$$\frac{\partial C_{\overline{M}}}{\partial r} \Delta r + \frac{\partial C_{\overline{M}}}{\partial \theta} \Delta\theta = 0 \ ,$$

and therefore,

$$\left.\frac{\Delta\theta}{\Delta r}\right|_{CG} = - \frac{\frac{\partial C_{\overline{M}}}{\partial r}}{\frac{\partial C_{\overline{M}}}{\partial \theta}} \ .$$

That is, the variation of attitude with gap is a direct measure of the ratio of the pitching moment derivatives in equilibrium flight at different lift coefficients. Thus, the location of the center of gravity essentially determines the attitude and gap variation which will occur as speed is changed.

At a different center-of-gravity position

$$C_{M_{CG2}} = C_{M_{CG1}} + \Delta\bar{x}\, C_L \ .$$

In equilibrium flight, $C_{M_{CG2}} = 0$, and therefore, at constant lift coefficient the change in the pitching moment coefficient about position 1 is

$$\frac{\partial C_{M_{CG1}}}{\partial r} \Delta r + \frac{\partial C_{M_{CG1}}}{\partial \theta} \Delta\theta = - \Delta\bar{x}\, C_L \ .$$

Thus, from the graph of lift coefficient vs. pitching moment coefficient the total quantity on the left hand side can be determined. Finding the corresponding points on the equilibrium curve of θ vs. r at the proper lift coefficient determines the change in θ and r to be inserted in the above relationship. This result is then employed, along with the ratio of the derivatives determined from the slope of the equilibrium curve, to

determine the pitching moment derivatives.

The above relationships are sketched graphically in Figure B-2. For simplicity, linear variations are sketched on this curve.

It should be noted that for different center-of-gravity positions the slope of the line representing the variation of θ with r, will change since

$$\left.\frac{\Delta\theta}{\Delta r}\right|_{CG} = - \frac{(C_{M_r} + \overline{\Delta x}\, C_{L_r})}{(C_{M_\theta} + \overline{\Delta x}\, C_{L_\theta})} \quad .$$

Since the following signs were found to be typical of the derivatives of this vehicle

$$C_{L_r} < 0 \ ,$$

$$C_{L_\theta} > 0 \ ,$$

$$C_{M_r} < 0 \ ,$$

$$C_{M_\theta} < 0 \ ,$$

moving the center of gravity aft ($\overline{\Delta x}$ positive) will cause the numerator of $\frac{\Delta\theta}{\Delta r}$ to increase and the denominator to decrease resulting in an increase in slope. The converse is true when the center of gravity is moved forward. The trend with center-of-gravity position is shown on Figure B-1.

It is interesting to note that in the case of a forward center-of-gravity location such that $C_{N_r} = 0$, the vehicle will fly at constant attitude as the speed varies. This would be indicated in Figure B-2 by the constant center-of-gravity position curve being

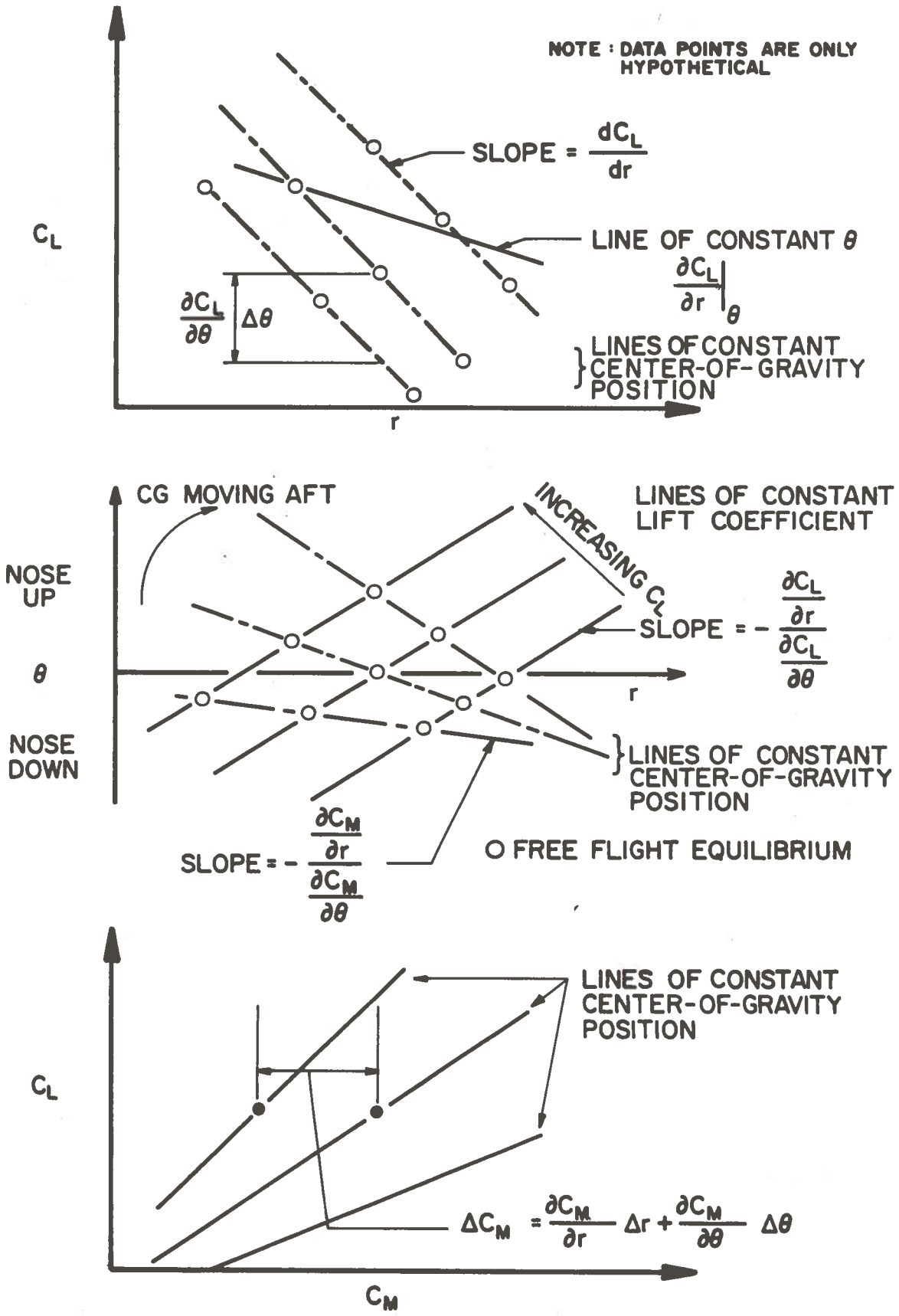

FIGURE B-2. STABILITY DERIVATIVE DETERMINATION, TOWED-MODEL TEST.

horizontal. This is almost the situation when the center of gravity is located at 0.4c for the model examined here at the smaller gaps as shown by the experimental data of Figures 18 through 20. As the gap increases, however, there is a definite increase in the downward slope. In the other extreme, with an aft center-of-gravity position such that, C_{M_θ} is equal to zero, that is, C_M is only a function of r, the line of constant center-of-gravity position will be vertical and as the speed of the vehicle varies, r will remain constant and the attitude will vary.

APPENDIX C

REPORT OF INVENTIONS

After diligent review of the work performed under this contract, no innovation, discovery, improvement, or invention of a patentable nature was made. The unconventional vehicle configuration which is described herein originated from previous efforts. The main contribution of the present effort was to supply quantitative test data on the dynamics of the concept.

*U.S. GOVERNMENT PRINTING OFFICE: 1977—702-132/287

110 copies

TRANSPORTATION SYSTEMS CENTER
KENDALL SQUARE, CAMBRIDGE, MA. 02142

OFFICIAL BUSINESS
PENALTY FOR PRIVATE USE, $300

POSTAGE AND FEES PAID
U. S. DEPARTMENT OF TRANSPORTATION
518